

Quantification of climate change impact on rainfall-induced shallow landslide susceptibility: a case study in central Norway

Emir Ahmet Oguz, Rasmus E. Benestad, Kajsa M. Parding, Ivan Depina & Vikas Thakur

To cite this article: Emir Ahmet Oguz, Rasmus E. Benestad, Kajsa M. Parding, Ivan Depina & Vikas Thakur (02 Jan 2024): Quantification of climate change impact on rainfall-induced shallow landslide susceptibility: a case study in central Norway, *Georisk: Assessment and Management of Risk for Engineered Systems and Geohazards*, DOI: [10.1080/17499518.2023.2283848](https://doi.org/10.1080/17499518.2023.2283848)

To link to this article: <https://doi.org/10.1080/17499518.2023.2283848>



© 2023 The Author(s). Published by Informa UK Limited, trading as Taylor & Francis Group



Published online: 02 Jan 2024.



Submit your article to this journal [↗](#)



View related articles [↗](#)



View Crossmark data [↗](#)

Quantification of climate change impact on rainfall-induced shallow landslide susceptibility: a case study in central Norway

Emir Ahmet Oguz ^{a,b}, Rasmus E. Benestad^c, Kajsa M. Parding^c, Ivan Depina^{a,d,e} and Vikas Thakur^a

^aDepartment of Civil and Environmental Engineering, Norwegian University of Science and Technology, Trondheim, Norway; ^bDepartment of Geotechnics and Natural Hazards, Norwegian Geotechnical Institute, Trondheim, Norway; ^cDepartment of Research and Development, Norwegian Meteorological Institute, Oslo, Norway; ^dDepartment of Rock and Soil Mechanics, SINTEF, Trondheim, Norway; ^eFaculty of Civil Engineering, Architecture and Geodesy, University of Split, Split, Croatia

ABSTRACT

Climate change impact on rainfall-induced landslide susceptibility of a certain region is often implied based on expected changes in rainfall patterns and rarely explicitly quantified. This study aims to address this gap by implementing coupled landslide and climate modelling chains to explicitly assess the effects of changing rainfall patterns on rainfall-induced landslide susceptibility. The effects of climate change are integrated into the landslide modelling chain via Intensity-Duration-Frequency (IDF) curves for the present and future climate conditions for a landslide-prone study area located in central Norway. The effects of climate change on landslide susceptibility are examined by using a physical-based landslide prediction model with rainfall events of varying duration and intensity that are simulated based on the climate-dependent IDF curves. The novelty of this study is the proposition of a novel probabilistic framework to assess the climate change impact on landslide susceptibility for rainfall events with a given duration. The proposed framework accounts for both the uncertainties of rainfall events through probabilistic interpretation of IDF curves and the uncertainties in the landslide model with the Monte Carlo method. Compared to results based on only intense rainfall events, the proposed framework leads to a lower increase in the probability of landslide initiation and landslide-susceptible extents due to climate change.

ARTICLE HISTORY

Received 20 December 2022
Accepted 20 September 2023

KEYWORDS


landslide susceptibility; rainfall; climate change; intensity-duration-frequency curves; probabilistic approach

1. Introduction

Climate change is an ongoing and unequivocal process (IPCC 2021). The emission of carbon dioxide (CO₂) and other greenhouse gases over time have caused global warming with increased temperature and more severe rainfall (IPCC 2012, 2021). In the Sixth Assessment Report (AR6) of the Intergovernmental Panel on Climate Change (IPCC), it is stated that the concentration of CO₂ in the atmosphere has increased by over 47% since 1750 and pre-industrial times (IPCC 2021). The magnitude of the expected climate change and the local consequences, such as long-term trends in precipitation, depend on the location and are strongly influenced by natural and stochastic regional variations associated with the atmospheric dynamics and the presence of various physical phenomena, such as cyclones, weather fronts, convection, and atmospheric rivers.

As extreme precipitation events are one of the most common triggering factors for landslides (Lacasse,

Nadim, and Kalsnes 2010; Pecoraro, Calvello, and Piciullo 2019), changes in climate, such as increasing total precipitation and precipitation intensity, may have a noticeable impact on landslide occurrence, frequency, and severity (Hanssen-Bauer et al. 2017). A large number of countries have performed country-specific or region-specific climate change predictions and the corresponding impact on landslide occurrence (Ho, Lacasse, and Picarelli 2017). Except for a few regions, the majority of the studies have reported an increase in air temperature, annual cumulative rainfall, and frequency of intense rainfall events until the end of the twenty-first century. These long-term changes in temperature and rainfall are expected to have profound impacts on both nature and society. A predicted increase in the frequency of landslide occurrence and associated risks to society have been reported by most of the countries, although the magnitude of the increase varies from region to region depending on the meteorological, environmental, and geomorphological factors controlling the landslide occurrence.

CONTACT Emir Ahmet Oguz  emir.ahmet.oguz@ngi.no

© 2023 The Author(s). Published by Informa UK Limited, trading as Taylor & Francis Group

This is an Open Access article distributed under the terms of the Creative Commons Attribution License (<http://creativecommons.org/licenses/by/4.0/>), which permits unrestricted use, distribution, and reproduction in any medium, provided the original work is properly cited. The terms on which this article has been published allow the posting of the Accepted Manuscript in a repository by the author(s) or with their consent.

Quantifying the impact of climate change on landslide susceptibility is important for mitigating the expected increase in societal risk from climate-driven rainfall-induced landslides (e.g. hazard mapping, emergency management, land use planning). Several researchers have investigated the ongoing climate change and its effects on geohazards, such as shallow landslides (e.g. Ciervo et al. 2017; Salciarini et al. 2019), slow active landslides (e.g. Comegna et al. 2013), reactivation of landslides (e.g. Dixon and Brook 2007) and deep-seated landslides (e.g. Rianna et al. 2014). Besides, Dehn et al. (2000) examined the displacement rates of the mudslides under climate change by employing hydrological and rheological models. In the study of Barik et al. (2017), the effects of climate change on landslide susceptibility were investigated for sustainable forest management. There exist studies on climate change impact on climatic abnormalities, such as typhoons, and corresponding effects on landslide occurrences (Chiang and Chang 2011; Shou and Yang 2015). These studies employed several methods linking climate change with landslide occurrence, such as physical-based models, statistical, and empirical methods. Among them, several studies investigated the effect of climate change on landslide susceptibility by employing a physical-based model with a rainfall event downscaled from global climate models (GCMs) and regional climate models (RCMs) (e.g. Chiang and Chang 2011; Melchiorre and Frattini 2012). To the extent of our knowledge, none of these abovementioned studies attempted to investigate climate change impact accounting for multiple rainfall events of the same duration, but mainly investigated rainfall events of different return intervals individually, especially extreme rainfall events of long return intervals (e.g. Melchiorre and Frattini 2012; Salciarini et al. 2019). However, considering only extreme rainfall events with a low probability of occurrence may overemphasise the climate change impact on landslide susceptibility.

In recent years, there has been significant progress in the development of physically based models for landslide susceptibility studies over large areas. These models take into account explicitly for physics, such as infiltration, and slope stability, rather than statistical and empirical methods to assess the susceptibility. There are several physical-based landslide susceptibility models, which have been employed at a local scale for a single slope or multiple slopes (up to 10 km²), or at a regional scale covering hundreds to thousands of km². Some of the commonly used physical-based models can be listed as dSLAM (Wu and Sidle 1995), SHALSTAB (Montgomery and Dietrich 1994), SINMAP (Pack et al. 2005), SLIP (Montrasio and Valentino 2008), GEOtop coupled with geotechnical models, for example, GEOtop-FS (Simoni

et al. 2008), TRIGRS (Baum, Savage, and Godt 2002, 2008), HIRESS (Rossi et al. 2013), and r.rotstab (Mergili et al. 2014). Among the references to physical-based models, TRIGRS (Transient Rainfall Infiltration and Grid-based Regional Slope-Stability analysis) has gained popularity due to accounting for excess rainfall due to soil saturation, unsaturated soil, and being less computational-demanding (e.g. Alvioli and Baum 2016; Ciarleo, Mandaglio, and Moraci 2019). Therefore, the current study employed the TRIGRS model for landslide susceptibility analysis.

This study focuses on quantifying the climate change impact on rainfall-induced landslide susceptibility with a modelling framework that includes climate and landslide modelling chains. In the modelling framework, climate change is represented by Intensity-Duration-Frequency (IDF) curves for the present and future climate conditions in a case study area located in Norway. IDF curves were selected as they allow us to describe the statistical properties of rainfall in a certain area. IDF curves also allow one to associate rainfall events of different durations and intensities with the likelihood of their occurrence, which is essential when conducting hazard or risk assessment of hazards that are triggered by rainfall events. In this study, a straightforward semi-empirical formulation (Benestad et al. 2021, 2019) was utilised to drive the climate-dependent IDF curves. This formulation provides a novel method for estimating the approximate values of rainfall depths for both daily and sub-daily rainfall events. The effects of climate change on landslide susceptibility are investigated by simulating rainfall events with varying durations and intensities based on the IDF curves from the climate modelling chain. Given the rainfall events, the uncertainties in the TRIGRS model parameters are propagated to the model predictions with the Monte Carlo method. The TRIGRS model predictions are presented in terms of probability of landslide initiation as a measure of landslide susceptibility. This study proposes a novel probabilistic framework to obtain an integrated climate change impact on landslide susceptibility. This is achieved by accounting for the likelihood of rainfall events with varying return intervals at a given duration. With the proposed probabilistic framework, the climate change impact on landslide susceptibility will be evaluated on a more reasonable basis by involving same-duration rainfall events of varying intensity, and not only based on extreme events with intense rainfall events.

Details of the modelling framework are presented in Section 2. Section 2.3 introduces the novel probabilistic framework. Section 3 provides a description of the study area. In Section 4, the future climate projections and landslide susceptibility maps are provided. Finally,

Section 5 addresses several discussion points, and Section 6 summarises the paper.

2. Methodology

The conceptual framework of the studies on the impact of climate change on landslides mainly involves the climate and landslide modelling chains (Alvioli et al. 2018; Gariano and Guzzetti 2016), with some studies also incorporating sensitivity analysis (Mtongori et al. 2015) and stress-testing (Benestad et al. 2019). The climate modelling chain might include different GCMs and RCMs, emission scenarios, and downscaling methods to assess future climate conditions. In the landslide modelling chain, physical-based, statistical, and empirical methods are used depending on, among others, landslide type, spatial and temporal scales. This section introduces the modelling framework that consists of coupled landslide and climate modelling chains. Implementation of the coupled modelling chains aims at capturing the complex interactions between, among others, climate, weather, and landslide processes.

Figure 1 shows the details of the modelling framework implemented in this study. The framework involves both climate and landslide modelling chains to project landslide susceptibility under climate change. The climate modelling chain investigates the present climate conditions and provides future climate projections. In this study, the present and future climate conditions are examined in terms of IDF curves by incorporating the simple formulation to estimate the approximate values of rainfall depths for daily and sub-daily rainfall proposed by Benestad et al. (2019, 2021). The details of the climate modelling chain are presented in Section 2.1. The landslide modelling chain employs a physical-based landslide susceptibility model, TRIGRS (Baum, Savage, and Godt 2008), to evaluate slope stability conditions across spatial and temporal scales (Section 2.2). The landslide susceptibility model is first calibrated based on the on-landslide inventory, geological, meteorological, and hydrological conditions over the study area. The outputs of the climate modelling chain, the climate-dependent IDF curves were utilised as an input to the calibrated landslide susceptibility model to evaluate the projected landslide susceptibility. The projected landslide susceptibility simulations are performed in a probabilistic framework that scales the impact of rainfall events proportionally to their probability of occurrence (see Section 2.3).

2.1. Climate modelling chain

GCMs are useful tools to simulate the response of the climate system to increased levels of greenhouse gases.

The Climate Model Intercomparison Project (CMIP), organised by the World Climate Research Programme (WCRP), has coordinated and provided common experimental protocols to climate modelling groups across the world (Eyring et al. 2016; Taylor, Stouffer, and Meehl 2012). The CMIP ensembles have been an important part of the scientific basis of the IPCC assessment reports (IPCC 2014, 2021). While GCMs offer a multifaceted view of the large-scale phenomena and processes in the atmosphere, they are unable to provide details on small-scale conditions. Hence, additional information is needed in order to study the local climatic response and consequences of a global climate change. The process of adding such information on smaller scales is known as downscaling (Benestad et al. 2016; Takayabu et al. 2016). One approach is to use empirical-statistical downscaling (ESD), which utilises information about the link between the large and small scales found in historical data. Another approach is dynamical downscaling, in which a RCM with higher spatial resolution is applied to a limited area, using GCM data as boundary conditions. In addition to these two, there is hybrid downscaling, which involves ESD that is trained on RCM data (Erlandsen et al. 2020).

The Coordinated Regional Climate Downscaling Experiment (CORDEX) provides a coordinated framework for climate downscaling (Jacob et al. 2014). While RCMs provide a versatile picture of the climate and can resolve many atmospheric processes and interactions, there are drawbacks to dynamical downscaling. RCMs may not be physically consistent with the GCMs from which they take their boundary conditions and RCM output tends to require bias correction before being used in impact studies. Because of the computational costs of dynamical downscaling, RCMs are typically applied to a limited number of GCM simulations and the small RCM ensembles may not provide an adequate sample of regional outlooks (Mezghani et al. 2019). Ideally, it is recommended to combine ESD and RCMs since they have different strengths and weaknesses independent of each other.

2.1.1. Precipitation data

Changes in the climate were examined based on the dynamically downscaled climate model data and historical observations of precipitation. The present climate condition was examined based on the historical observations of precipitation, while the projections of precipitation from climate model simulations were combined with the historic observations to obtain the future climate conditions. Daily precipitation data for climate projections are obtained from dynamically

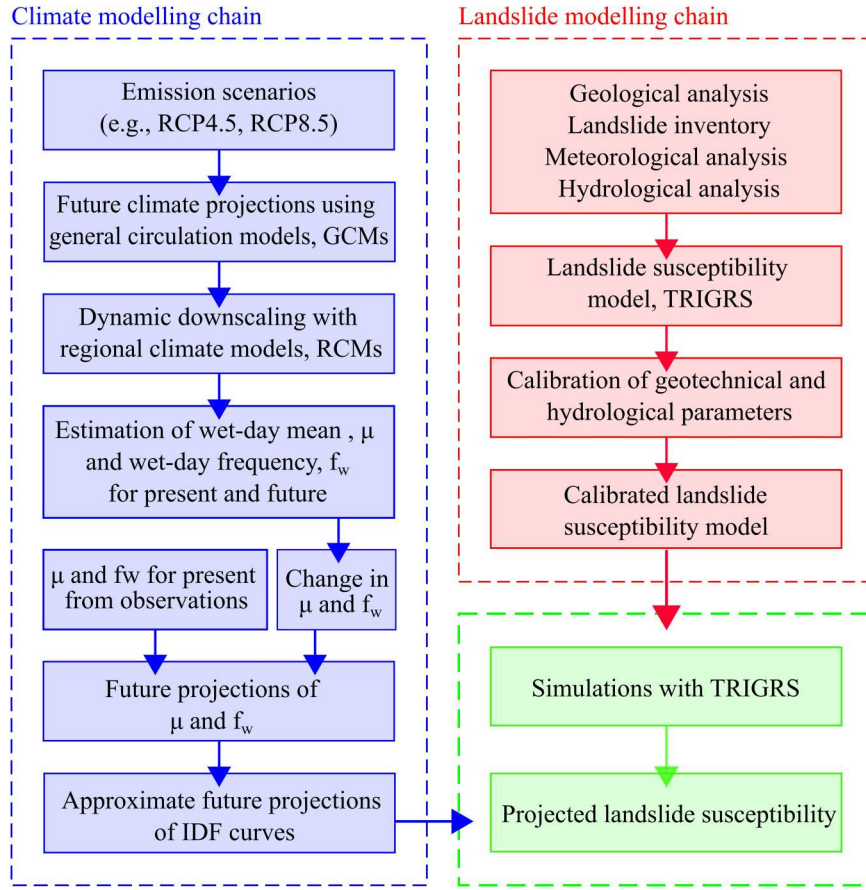


Figure 1. Modelling framework including climate and landslide modelling chains. The variables μ represents the wet-day mean precipitation whereas f_w refers to the wet-day frequency.

downscaled high-resolution CORDEX simulations for Europe (EUR-11) (Jacob et al. 2014). The data ensemble consists of 56 projections, which combine 22 RCMs with a spatial resolution of 0.11° (≈ 12.5 km) that are applied to the output from 8 different GCM simulations from CMIP5 (Taylor, Stouffer, and Meehl 2012). There are inter-dependencies between the different RCM runs, both due to common boundary conditions provided by the same GCM and repeated RCM models with specific biases. The spread nevertheless gives some indication about the level of uncertainty associated with these results, keeping in mind that such a small number of GCM simulations may not represent the whole range of possible outcomes (Mezghani et al. 2019). Additionally, historic precipitation data were obtained from the weather stations and retrieved from the Norwegian Meteorological Institute using the Frost application programming interface (MET n.d.).

2.1.2. Intensity-duration-frequency calculations

A simple semi-empirical formula was used to calculate approximate daily and sub-daily rainfall statistics in

terms of IDF curves (Benestad et al. 2021):

$$x_L = \alpha \mu \left(\frac{L}{24} \right)^\zeta \ln(f_w \tau) \quad (1)$$

where x_L is the return level, i.e. rainfall depth, (in mm) associated with rainfall duration L (in hours), τ is the return interval, μ is the wet-day mean precipitation (in mm/day) and f_w is the wet-day frequency ($f_w \in [0, 1]$). The values for α and ζ reflect how the daily rainfall statistics diverge from an exponential distribution and how the different time scales are connected, respectively. They are approximately constant in Norway, whereas μ and f_w reflect the local rainfall statistics that to a greater extent vary both geographically and temporarily.

Here, μ and f_w were calculated based on daily precipitation data using a threshold of 1 mm/day to define a “wet-day”. f_w was calculated as the fraction of days in a month above the threshold and μ as the mean precipitation on those wet days. IDF curves were estimated for two time horizons: 1981–2010 and 2071–2100, using the values of μ and f_w applied to Equation (1). For the present day, the rainfall depths were calculated using all

available observational data in the reference period. For the future period, the rainfall depths were calculated using the observed mean values of μ and f_w for the present day, and then adding the projected changes in μ and f_w from the present day to the future period, which were calculated based on RCM simulations.

2.2. Landslide modelling chain

Landslide prediction over large areas often depends on establishing a functional relationship between meteorological conditions and slope stability. The relationship can be developed and implemented with several approaches such as simple rainfall–landslide relationship based on a threshold level (Ciervo et al. 2017; Sangelantoni, Gioia, and Marincioni 2018), empirical methods including several factors associated with landslides (Dixon and Brook 2007; Shou and Yang 2015), machine learning models (Chang et al. 2020; Huang et al. 2020a, 2020b, 2020c; Kainthura and Sharma 2022; Su et al. 2022; Xiao et al. 2022), or physical-based models (Alvioli et al. 2018; Chiang and Chang 2011; Melchiorre and Frattini 2012; Salciarini et al. 2019; Scheidl et al. 2020). Among these methods, physical-based models are widely utilised as they generally incorporate hydrological and geotechnical processes explicitly into the landslide modelling. These models can be utilised for spatial and temporal prediction of landslide initiation, or for landslide susceptibility assessment. TRIGRS was applied in this study as one of the most commonly used models (e.g. Ciurleo, Mandaglio, and Moraci 2019; Park, Nikhil, and Lee 2013; Weidner et al. 2018).

The calibration of physical-based models is a crucial step for landslide susceptibility analysis, as it allows for more reliable predictions. A calibration strategy can be selected based on the available information and advanced calibration methods (e.g. Depina, Oguz, and Thakur 2020; Luo et al. 2022) can be utilised. In this study, the calibration strategy of the TRIGRS model was selected and implemented by considering the collected information over the study area on geology, landslide inventory, meteorological conditions, and hydrological conditions. The details of the calibration will be provided in Section 3.4.

2.2.1. TRIGRS model

TRIGRS is a Fortran code developed to obtain the spatial and temporal distribution of rainfall-induced shallow landslide occurrence over large areas (Baum, Savage, and Godt 2002, 2008). The model couples a hydrological infiltration model, a model for routing of runoff, and an infinite slope stability model to

examine the response of large areas to rainfall events. The TRIGRS is a cell-based model where the calculations for the infiltration and slope stability are performed on cell-by-cell basis, i.e. individually for each cell over the discretised domain.

The hydrological infiltration model is based on analytical solutions to the one-dimensional Richards equation describing the vertical movement of water through the soil medium. This study assumed saturated initial condition in TRIGRS model. Accordingly, the solution for the transient pore pressure head, $\psi(Z, t)$ (Equation (2)) superposes the steady long-term, $\psi_0(Z)$, and transient short-term response, $\psi_1(Z, t)$, to a rainfall event.

$$\psi(Z, t) = \psi_0(Z) + \psi_1(Z, t) \quad (2)$$

where Z is the vertical depth from the ground surface and t is the time. The steady long-term component is a function of Z , initial ground water depth vertically from ground surface, d , slope angle, δ , long-term vertical infiltration rate, I_{ZLT} , and hydraulic conductivity, K_S (Equation (3)).

$$\psi_0(Z) = (Z - d)[\cos^2(\delta) - I_{ZLT}/K_S] \quad (3)$$

For the transient short-term component, TRIGRS provides solutions for two subsurface conditions: an infinite depth basal boundary and an impermeable basal boundary at finite depth. In case of having a relatively uniform hydraulic property through depth, the solution for a subsurface condition with a basal boundary at an infinite depth applies. However, the other solution applies where there is an impermeable basal boundary at a finite depth or a high contrast in hydraulic property through depth. In this study, the solution for infinite depth basal boundary was employed in the model. The formulation for the transient short-term component can be found in TRIGRS manual (Baum, Savage, and Godt 2008). The hydrological infiltration model may result in unrealistic pressure heads at shallow depths (Iverson 2000). Therefore, calculated pressure heads are restricted by $\psi(Z, t) \leq Z[\cos^2(\delta) - (I_{ZLT}/K_S)]$ in the model.

The TRIGRS model routes the excess rainfall water due to soil saturation or the exceedance of infiltrability of the soil. The excess rainfall water is routed to downslope to the adjacent cells, proportional to the weighing factors assigned to the adjacent cells.

TRIGRS employs an infinite slope stability model calculating the factor of safety of a slope, F_S , as a ratio of the resisting to driving forces:

$$F_S(Z, t) = \tan \phi' / \tan \delta + (c' - \psi(Z, t)\gamma_w \tan \phi' / (\gamma_s Z \sin \delta \cos \delta)) \quad (4)$$

where c' is the effective cohesion, ϕ' is the effective friction angle, γ_w and γ_s are unit weight of water and soil

respectively, and δ is the slope angle. Slope stability assessment is conducted along the depth, and the minimum F_S is provided. A slope is considered to be stable if $F_S > 1.0$ and unstable if $F_S \leq 1.0$.

2.2.2. Uncertainties in model parameters

The uncertainties in the geotechnical and hydrological parameters have been reported in the literature (Baecher and Christian 2003; Fenton and Griffiths 2008; Phoon and Kulhawy 1999). The lack of knowledge on the parameters and the inherent natural variability due to the varying deposition and formation processes in geological history are mainly accepted as sources of the uncertainty. Avoiding this uncertainty and employing deterministic values for the geotechnical and hydrological parameters may result in conservative or unrealistic results.

Several studies have accounted for the variability of the model parameters in physical-based landslide modelling (e.g. Arnone et al. 2016; Melchiorre and Frattini 2012; Raia et al. 2014; Rossi et al. 2013; Scheidl et al. 2020). Among them, Raia et al. (2014) reported improvement of the predictive capacity of the TRIGRS model when the variability of the model parameters is accounted in the model simulations. In this study, TRIGRS model has been coupled with Monte Carlo method due to its robustness and straightforward implementation. The uncertainties in the model parameters are propagated to the model output in terms of F_S by performing 1000 Monte Carlo simulations. The TRIGRS model simulation outputs were utilised to evaluate the probability of landslide initiation for a given value of rainfall duration and intensity, $P_f(L, I)$, which is calculated as:

$$P_f(L, I) = P(F_S \leq 1.0 | L, I) = \frac{1}{N_S} \sum_{i=1}^{N_S} \lambda(F_{S,i} - 1.0) \quad (5)$$

where L and I are duration and intensity of the rainfall event, N_S is the number of simulations, $F_{S,i}$ is the factor of safety of i^{th} simulation, and λ is the indicator function providing 1 if $F_{S,i} - 1.0 \leq 0$, and 0 otherwise.

2.3. Probabilistic framework

The effects of climate change on landslide susceptibility have been mainly evaluated under extreme conditions such as intense rainfall events with long return intervals (e.g. Melchiorre and Frattini 2012; Salciarini et al. 2019; Scheidl et al. 2020; Shou and Yang 2015). However, these extreme events have low probability of occurrence and may result in misleading assessment of climate change impact on landslide susceptibility.

Accounting for the probability of occurrence of rainfall events can provide a better understanding of climate change impact. Therefore, there is a need for a probabilistic framework to account for the probability of occurrence of rainfall events with varying return intervals to understand climate change impact on landslide susceptibility.

This study proposes a probabilistic framework to account for the probability of occurrence of rainfall events and obtain a comprehensive climate change impact on landslide susceptibility. The proposed framework is advantageous as it integrates the results from both the landslide and climate modelling chains in a consistent approach and provides an integrated climate change impact of multiple rainfall events of the same duration. The resulting estimate is the probability of landslide initiation for a given value of rainfall duration, $P_f(L)$, calculated as follows:

$$\begin{aligned} P_f(L) &= P(F_S \leq 1.0 | L) \\ &= \iiint P(F_S \leq 1.0 | L, I) f(I | \mu, f_w, L) f(\mu, f_w) dI d\mu df_w \end{aligned} \quad (6)$$

where $P(F_S \leq 1.0 | L, I)$, i.e. $P_f(L, I)$ is the probability of landslide initiation conditioned on L and I values, $f(I | \mu, f_w, L)$ is the probability density function (pdf) of rainfall intensity conditioned on the values of μ , f_w , and L , and $f(\mu, f_w)$ is the likelihood of a given pair of μ and f_w based on data ensemble of CORDEX simulations for Europe. Distribution of $\mu - f_w$ pairs for climate projections was modelled by Gaussian distribution using the 56 projections. $f(I | \mu, f_w, L)$ was modelled by the Gumbel distribution, with the distribution parameters determined by fitting the distribution to the intensity values provided by the climate model based on μ and f_w for a given value of L .

The landslide susceptibility analyses were performed for intensity values for a given duration, which were obtained by discretizing the range of intensity values in the climate-dependent IDF curves. Then, Equation (6) was utilised to integrate the results, $P_f(L, I)$, over rainfall intensity and obtain $P_f(L)$ for both present and future climate conditions for a given value of L .

3. Study area

The study area (11.2304 – 11.7571°E/63.3594 – 63.5144°N) is located in Trøndelag, central Norway Figure 2(a). It covers around 200 km² of the catchment of the Stjørdal river Figure 2(b) that flows from the Swedish border on the east and discharges into the Trondheim Fjord on the west.

3.1. Weather conditions

In the report of “Climate in Norway 2100” (Hanssen-Bauer et al. 2017), the climate observations in Trøndelag, central Norway show that the mean air temperature increased by ca. 0.1°C per decade since 1900. In the period of 2000–2021, the average mean air temperature is approximately 4.9°C and may typically vary from –30°C to +34°C in a year.

There are two weather stations in operation, one on the east and one on the west of the study area. The weather station on the east is in operation since 2004 and therefore has limited available data. The station on the west, Østås i Hegra (station id: 69550, 11.3536°E/63.4871°N) is in operation since 1895 and has reliable and long observation data. Therefore, for the climate projections, daily precipitation observations from the station Østås i Hegra were utilised.

Based on the historical observations of precipitation from station Østås i Hegra, there has been an increasing trend in annual μ of the order of 0.002 mm/day per year consistent with an increase from 6.8 mm/day in 1900 to 7.1 mm/day in 2020. Similarly, there has been an increase in f_w on the order of 0.0003 per year, from 0.39 in 1900 to 0.43 in 2020.

3.2. Geology

The study area is underlined by the bedrock composed of Proterozoic and Cambrian metamorphic rocks deformed during the Caledonian orogenesis. There exists a layer of Quaternary deposits of different origin covering the bedrock. Based on the available geological map from the Geological Survey of Norway (NGU n.d.), the Quaternary deposits include glacial deposits (moraine), marine deposits below the marine limit in the proximity of the Stjørdal river, river – stream (fluvial) deposits, fluvial material transported and deposited by glaciers (glaciofluvial deposits), loose masses formed by physical and chemical degradation of the bedrock, thin peat and humus cover over bedrock, and bedrock outcrop. Fluvial and glaciofluvial deposits have the same material composition with different phenomena in transportation and deposition history. Additionally, marine deposits also have similar composition of fluvial deposits and only exist occasionally near the river with small extents. Therefore, the fluvial deposits, glaciofluvial deposits, and marine deposits have been grouped as “fluvial deposits” for simplicity. Similarly, the bedrock outcrop and loose masses formed by the physical and chemical degradation of the bedrock have been grouped as “rock”. Figure 2(d) shows the

Quaternary map of the study area including four geology units: moraine deposits, fluvial deposits, humus–peat, and rock.

The moraine deposits were picked up, and transported by glaciers. These deposits are generally hard-packed, poorly sorted, and may contain anything from clay to rock. The thickness varies from very thin, 0.2 m, to a few metres or even more. The fluvial deposits have sorted and rounded sand – gravel dominated composition, and mainly located along the Stjørdal river. Generally, a thick cover of fluvial deposits, from 0.5 m to more than 10 m, does appear in the study area. The humus – peat has high organic content due to roots and plants, and generally exists as a thin cover, less than 0.5 m over the bedrock. Finally, the rock type includes bedrock crops and weathered rocks. NGU reported the infiltration rates as varying from very poor to poor in the deposits that cover the hillslopes (e.g. moraine), while there is a relatively good infiltration capacity in the deposits covering the bottom of the valley (e.g. fluvial deposits).

Due to the TRIGRS model being applicable to soil-related landslides, this study focuses on moraine and fluvial deposits, but not rock and humus–peat. The moraine and fluvial deposits cover 40% of the study area Figure 2(d), with 32% being moraine and 8% being fluvial deposits. The average slope angle over the moraine area is 14.7° while it is 10.2° for the fluvial deposits as the fluvial deposits are mainly located along the Stjørdal river. Additionally, the extent of the moraine with a slope angle greater than 30° is 4.2 km², while it is 0.9 km² for the fluvial deposits.

3.3. Landslide inventory

The elevation of the study area was obtained from the map service “hoydedata.no” from the Norwegian Mapping Authority (Kartverket n.d.) and ranges from 23.5 m to 1109.6 m with a bumpy topography. Slope angles and direction of runoff were derived from the digital elevation model (DEM) with a resolution of 10 m. Very steep slopes can be found along the Stjørdal river with slope angles greater than 30° Figure 2(c). The study area was reported to have very high landslide susceptibility by the Norwegian Water Resources and Energy Directorate, NVE (Devoli, Bell, and Cepeda 2019).

The national database of mass movements of Norway, “skredregistrering.no” (NVE n.d.) was investigated for the study area. The mass movements in the database include rockfalls, stone slides, snow avalanches, debris flow – avalanches, clay slides, icefalls, and slides on the road fill. In the study area, 93 registered mass

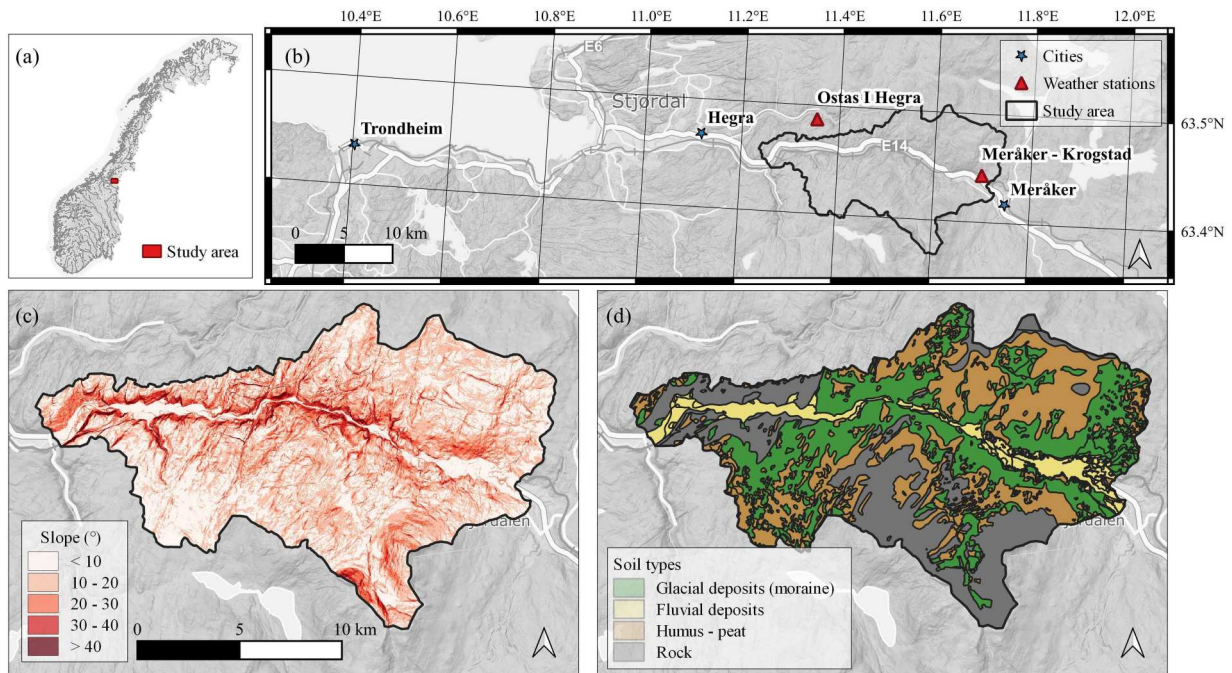


Figure 2. Location of the study area in (a) national scale, (b) Trøndelag, central Norway, with (c) slope and (d) geology maps.

movements were registered, located mainly along the main transportation lines. Among these registered mass movements, 35 events are classified as landslides in soil and were triggered by rainfall, snow-melting, or a combination of these two. These landslide events were reported to be shallow, and the volumes were estimated in the range of 5–50 thousand m^3 . Among them, 16 landslide events have polygonised source and runoff zones that were obtained by evaluating the aerial

pictures over time and field surveys. Figure 3 shows the landslide domain over the study area with two zoomed-in locations showing examples of polygonised landslide events. Figure 3a shows also the susceptibility levels at catchment scale (Devoli, Bell, and Cepeda 2019) by the logistic regression method and the zones susceptible to debris flow (Fischer et al. 2012) by using an index-based approach considering topographic characteristics.

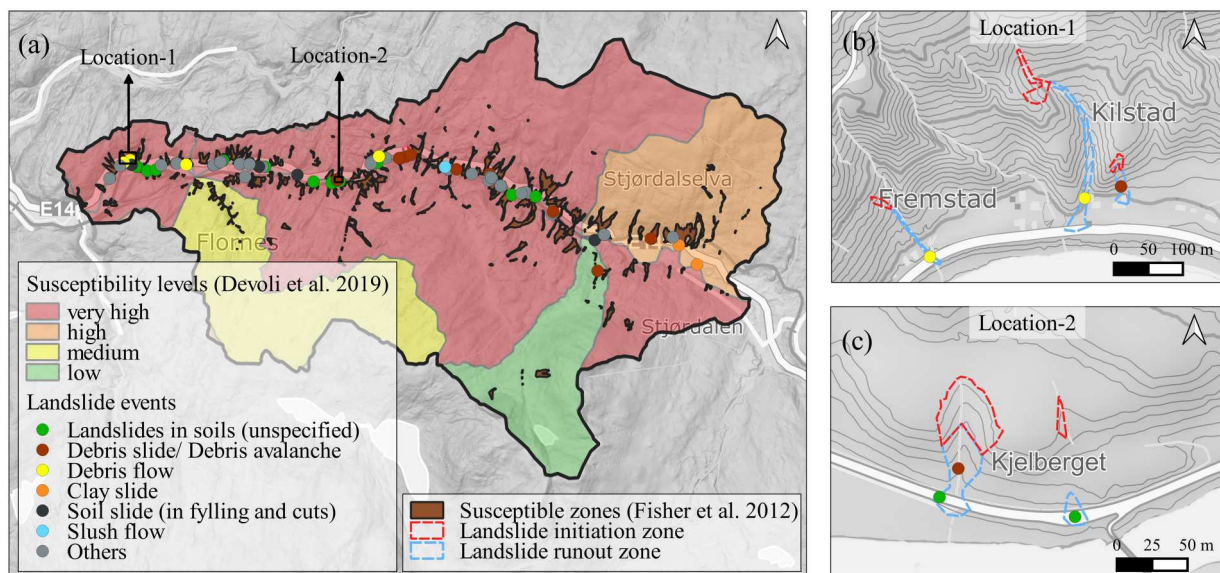


Figure 3. (a) Landslide domain over the study area in Trøndelag, central Norway, with two zoomed-in locations: (b) location-1 and (c) location-2.

Moreover, the landslide events were further filtered considering the quality of registration, date of occurrence (events after 2000), position and time, registration accuracy, and weather conditions on the date of occurrence. Following the filtering of events, 19 events were found to be convenient for the scope of the current study. Among the 19 landslide events, 14 events have polygonised initiation zones. For the remaining 5 events, possible initiation zones were located considering the descriptions in the national database and the topographic characteristics of the study area. A point with a 20 m buffer zone was placed on the possible initiation zone to be used in the TRIGRS model calibration.

Among the 19 events, 13 events are in fluvial deposits, and 3 events are in moraine. The remaining 3 events overlap both soil types. The initiation zones of the 19 landslide events include varying degrees of slopes from soft ($0\text{--}10^\circ$) to very steep ($> 40^\circ$), with 29.2° being the median. Five landslide events do not have cells with a slope greater than 30° . The spatial extent of the 19 landslide events varies from 500 to 3700 m^2 , with 1615 m^2 being the average.

The meteorological and hydrological conditions for the landslide events were determined by utilising the observations at the nearby weather stations and the national web portal, “xgeo.no” (Xgeo n.d.) which is a tool for visualising spatial and temporal data including observations, model simulations, forecasts, and real-time data. The 19 events occurred between 2000 and 2019, mainly in the periods of February – March and August – September. The analysis of hydrometeorological conditions revealed that the selected landslides were triggered by intense rainfall in the period of August – September, or by the combination of intense precipitation and some snow melting in the period of February – May. The average water supply was 49.8 mm/day in the range of $\{11.9, 82.0\}$. The degree of soil saturation data provided by Xgeo shows that the average degree of soil saturation was 79.1% with a minimum of 49% and a maximum of 99% . The reported percentages for degree of soil saturation describe the relationship between the soil water storage compared to the maximum soil water storage simulated by the rainfall-runoff HBV model (Beldring et al. 2003) in the reference period 1981–2010. Additionally, the ground water table levels on the day of landslide events were also reported to be very high compared to the normal levels for most of the events. The pictures of the landslide deposits in the runout zones also revealed the high water content in the sliding mass.

3.4. Calibration of landslide model parameters

In the calibration process, a conventional deterministic approach was implemented with the parameters assumed to be constant for each geological unit as a compromise between the accuracy and high computational demands of a probabilistic calibration (Depina, Oguz, and Thakur 2020). Considering the degree of saturation ratio values, and the ground water levels for the 19 landslide events, the soil was assumed to be fully saturated with a ground water table at the ground surface at the time of landslide initiations, i.e. after rainfall. Additionally, fully dry condition was assumed for before rainfall condition when all study area should be stable. The possible ranges of geotechnical strength parameters, i.e. cohesion and friction angle for fluvial deposit and moraine, were determined by considering the literature (Depina, Oguz, and Thakur 2020; Melchiorre and Frattini 2012) and the definitions of the soil types by NGU. For the fluvial deposit, low cohesion values, $1\text{--}5\text{ kPa}$, with a friction angle in the range of $39\text{--}43^\circ$ were examined. Similarly, for the moraine, the cohesion and friction angle parameters were examined in the ranges of $3\text{--}9\text{ kPa}$, and $29\text{--}36^\circ$. The parameter ranges were discretised into integer values and all sets of parameters were determined from the combination of the discretised values.

Some of the commonly used metrics to evaluate the performance of the model are provided in Fawcett (2006) and include false/true positive (FP/TP), true/false positive rate (TPR/FPR), accuracy, precision. Similarly, the success rate, the Kappa value, and modified success rate are other metrics used in the literature (Huang and Kao 2006). For the performance evaluation, this study employed an objective function, which accounts for both the stability of the study area before and after a rainfall event and capturing the landslide initiation zones. The objective function, f_{obj} (Equation (7)) accounts for: (i) the ratio of the number of initiated landslides to the total number of landslide events before the rainfall event; (ii) the ratio of the number of missed landslide events to the total number of landslide events after rainfall event; and (iii) the FPR after the rainfall event. The lower the value of f_{obj} , the better the performance of the model is.

$$\begin{aligned}
 f_{obj} = & \left[\frac{\sum_{i=1}^{N_l} \lambda(\min(F_{S_j}; j = 1, \dots, k) - 1.0)}{N_l} \right]_{\text{before rainfall}} \\
 & + \left[1 - \frac{\sum_{i=1}^{N_l} \lambda(\min(F_{S_j}; j = 1, \dots, k) - 1.0)}{N_l} \right]_{\text{after rainfall}} \\
 & + c(FPR)_{\text{after rainfall}}
 \end{aligned} \tag{7}$$

where N_l is the number of initiation zones of the landslide events, F_{Sj} is the factor of safety of cell j inside the landslide i , k is the total number of cells inside landslide i , c is the importance weight of predicting the stable zones after the rainfall event, and λ is the indicator function. FPR is the ratio of cells predicted as unstable outside of the discretised landslide zone (FP) to the number of cells without landslide observation (N) and calculated as $FPR = FP/N$.

The criteria in the calibration procedure is that the landslide events should be stable before rainfall and predicted after rainfall, and the zones outside of the discretised landslide initiation zone should be stable after rainfall. The coefficient c adjusts the stability of the study area after the rainfall event. As the coefficient c increases, the study area becomes more stable with a lower FP after rainfall. At a certain value of c , the set of parameters providing the best performance gives zero FP after rainfall. At this point, the balance between over- or under-predicting the stable zone and capturing the landslide events is accepted to be achieved. Then, the set of parameters resulting in the lowest F_S over the landslide initiation zones is selected.

TRIGRS simulations were performed for each set of parameters to determine the optimal geotechnical strength parameters of fluvial deposit and moraine type of soils with the model performance being evaluated by f_{obj} . The coefficient c in Equation (7), increased from zero to a certain value providing zero FP after rainfall for the set of parameters providing the best performance. In case of having several sets of parameters providing the same value of f_{obj} with zero FP , the set of parameters giving the lowest F_S for the landslide initiation zones was selected. Following the performance evaluation of all sets of parameters, cohesion and friction angle were selected as 6 kPa and 35° for moraine, and 5 kPa and 40° for the fluvial deposits. The assigned parameters are also in great agreement with the geotechnical strength parameters obtained by large-scale direct shear tests (Oguz et al. 2022).

The performance of the calibration process based on Equation (7) was found to be satisfactory. After the calibration, the whole study area including both the cells with landslide and non-landslide observation is stable before rainfall, and all landslide events, except 5 landslide events having no cells with a slope greater than 30° , are captured after rainfall (i.e. having a factor of safety of 1). The minimum factor of safety of the cells in the 5 non-captured landslide initiation zones ranges between 1.1 and 1.5. An accuracy of 99% was achieved after rainfall, but mainly due to the landslide inventory being incomplete over the study area, and lack of information on initial conditions.

Table 1. Model parameters.

Parameter	Distribution	Moraine	Fluvial deposit	CoV
Depth to bedrock, H (m)	–	$5.0 \exp(-0.04\delta)^a$		0.25
Unit weight, γ (kN/m ³)	Normal	20	19	0.02
Cohesion, c (kPa)	Lognormal	6	5	0.3
Friction angle, ϕ ($^\circ$)	Normal	35	40	0.1
Saturated permeability, K_S (m/s)	Lognormal	$5.0 \cdot 10^{-5}$	$1.0 \cdot 10^{-4}$	0.25
Diffusivity, D_0 (m ² /s)	Lognormal	$2.5 \cdot 10^{-3}$	$5.0 \cdot 10^{-3}$	0.25

^aSlope, δ is in degrees.

In this study, the hydrological parameters were not estimated in this calibration process as the infiltration does not change the transient pore pressure response at fully saturation condition, and not accounted for at dry condition. Instead, a parametric hydrological analysis was performed via TRIGRS model to investigate the response of soils with varying hydrological parameters to the present and future IDF curves (Appendix A). The hydrological parameters of two soil types: fluvial deposit and moraine were determined by considering the literature (Depina, Oguz, and Thakur 2020; Melchiorre and Frattini 2012), the hydrological characteristics reported by NGU, and the parametric hydrological analysis. The K_S for moraine and fluvial deposit have been selected as $5.0 \cdot 10^{-5}$ and $1.0 \cdot 10^{-4}$ m/s, respectively. Additionally, the ratio of D_0/K_S was decided as 50 to avoid too slow or fast pore pressure build-up.

Table 1 shows the calibrated geotechnical strength parameters and selected hydrological parameters for the geological units, moraine and fluvial deposits. In this study, the humus–peat and rock units were omitted from the analyses. Due to the lack of field data on depth to bedrock, H (m), it was calculated by an empirical relationship between the depth and slope inclination in degree, $H = 5.0 \exp(-0.04\delta)$ (Baum, Godt, and Savage 2010). While such empirical relationships are often used in regional landslide susceptibility analyses, their accuracy may be limited. The variability levels of the model parameters, i.e. CoV, were assigned considering the values in the literature (Depina, Oguz, and Thakur 2020; Melchiorre and Frattini 2012; Phoon and Kulhawy 1999), and used only for moraine and fluvial deposits in the TRIGRS model simulations. Cross-correlation among the soil parameters (e.g. Javankhoshdell and Bathurst 2016) is not accounted for in the probabilistic landslide susceptibility analyses.

4. Results and discussion

4.1. Future climate projections

In this study, the high emission scenario, representative concentration pathway (RCP), RCP8.5, based on the

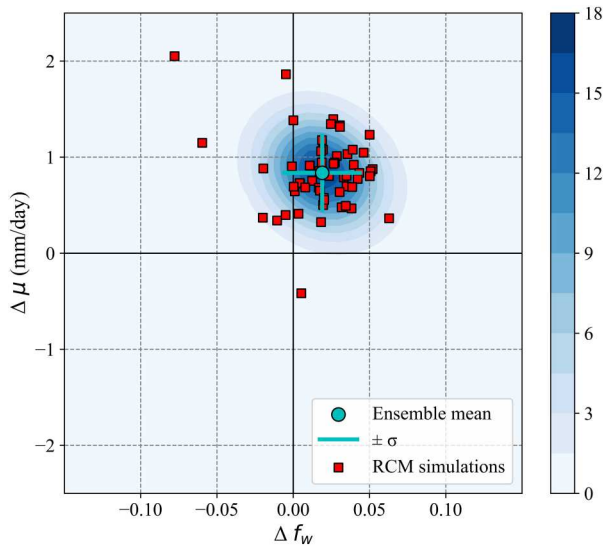


Figure 4. Projected changes in the wet-day mean precipitation (μ) and frequency (f_w) from a reference period (1981–2010) to the future (2071–2100) with the fitted bivariate Gaussian distribution.

assumptions of no climate policy, was investigated and the corresponding Euro-CORDEX ensemble was utilised. Figure 4 displays the projected change in wet-day mean precipitation (μ) and frequency (f_w) in Equation (1), from the period of 1981–2010 to the end of the century (2071–2100), based on the Euro-CORDEX ensemble. For each simulation, the grid point of the Euro-CORDEX data closest to the weather station, Østås i Hegra, was selected. From Figure 4, it can be seen that most of the RCMs of the Euro-CORDEX ensemble simulated increases in both μ and f_w with further global warming, both of which are key parameters of Equation (1). The results revealed the variability in the projections by the RCMs in the ensemble. The projected changes in μ and f_w , by the ensemble

mean, are 0.836 mm/day (σ : 0.387) and 0.0189 day/month (σ : 0.0248), respectively.

A bivariate Gaussian distribution was fitted to the projected changes in μ and f_w by assuming independence between the parameters (Figure 4). The goodness of fit of the Gaussian distribution was evaluated with 56 pairs of μ and f_w using a chi-squared test. The test yielded a chi-square value of 7.5 with 36 degrees of freedom and a p -value of 0.83, indicating that the data is consistent with a Gaussian distribution, and can be used to model the relationship between μ and f_w .

Figure 5 shows the 10-, 50- and 100-year IDF curves for the present climate calculated from observations (blue solid line), and ensemble statistics for the end of the century estimated from the Euro-CORDEX ensemble combined with the observations. While red solid lines show the ensemble mean, the dashed lines show 5th and 95th percentiles. The results suggest a considerable increase in the rainfall depths for all return intervals. There is some spread within the Euro-CORDEX ensemble, but even the 5th percentile indicates an increase compared to the present day, which makes sense as the majority of models projected an increase in both μ and f_w (Figure 4).

Figure 6 shows the IDF curves representing the present climate conditions based on observations, and future projections based on the mean projected change by the Euro-CORDEX ensemble combined with the observations, for a range of return intervals (2, 5, 10, 50, 100 and, 200 years). The climate-dependent IDF curves are presented as rainfall depth in Figure 6(a) and as rainfall intensity in Figure 6(b) by dividing the rainfall depths by the corresponding rainfall durations. The results showed that the rainfall depths increase by a mean factor of 1.128 ($\in [1.126, 1.130]$) due to climate change.

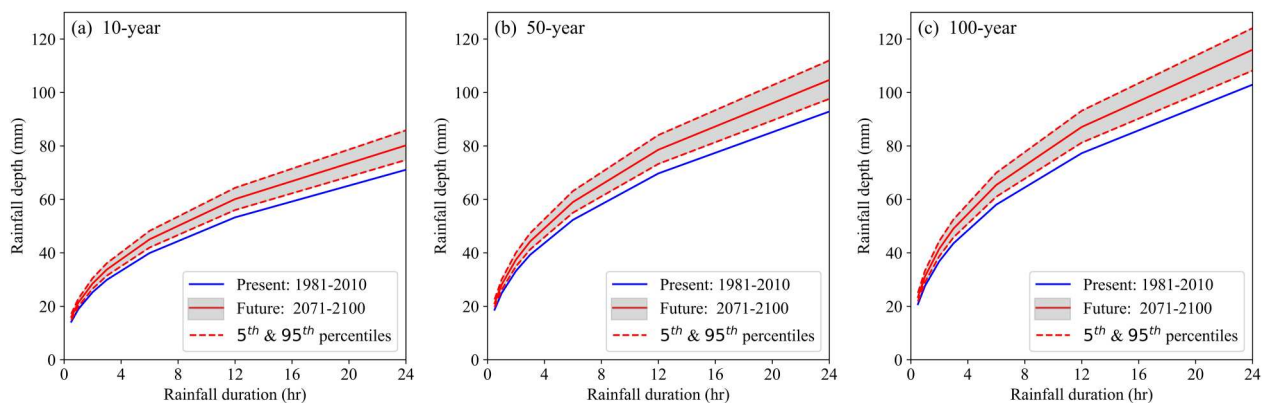


Figure 5. Estimated rainfall depths for (a) 10-, (b) 50-, and (c) 100-year return intervals based on RCM simulations from EURO-CORDEX assuming emission scenario RCP8.5.

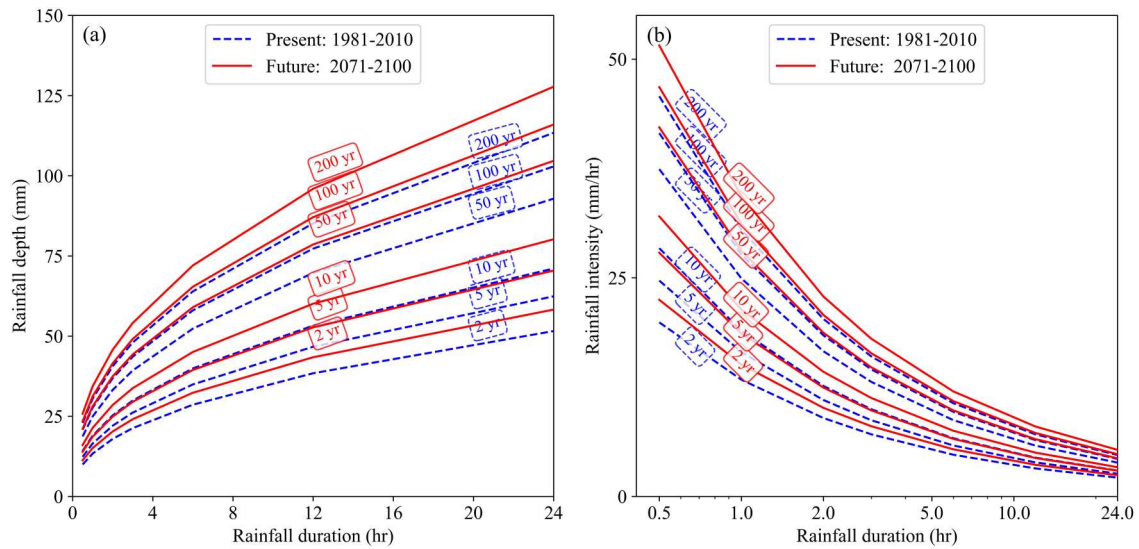


Figure 6. Estimated rainfall depths for Østås i Hegra weather station based on RCM simulations from EURO-CORDEX assuming emission scenario RCP8.5 (a) and rainfall intensities (b).

4.2. Projected landslide susceptibility

For the landslide susceptibility analyses, the initial ground water table was assumed at the bottom of the soil layer, and the rainfall events were simulated as a

uniform spatial event during rainfall duration. The landslide susceptibility analyses were conducted over the entire study area (Section 3) and corresponding statistics of the probability of failures, $P_f(L)$ and $P_f(L, I)$, are provided. Just for visual inspection, these values of

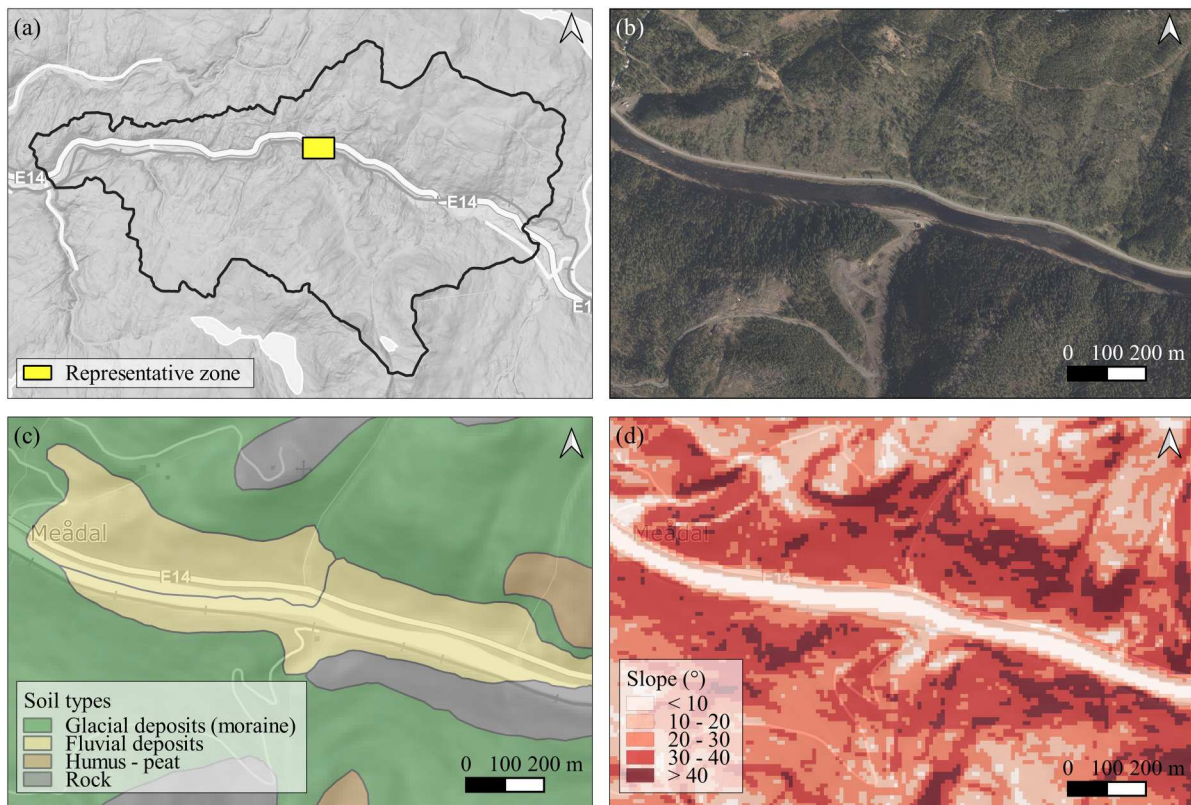


Figure 7. The representative zone for the illustration of climate change impact: (a) regional scale, (b) aerial photo, (c) geology and (d) slope maps.

probability are provided over a representative zone Figure 7(a) in Figures 8–10 due to study area being too large. On closer inspection in Figure 7, it can be seen that the representative zone has both soil types of interest Figure 7(c) and steep slopes can be found in areas with both soil types Figure 7(d).

This section will present, first, climate change impact on the response of the study area to different rainfall durations by providing $P_f(L)$ maps obtained by the proposed probabilistic framework (Section 2.3). This framework utilised 1000 pairs of μ and f_w , which were drawn from the bivariate Gaussian distribution for the projected changes in μ and f_w in Figure 4, and associated climate-dependent IDF curves. Secondly, the climate change impact for the rainfall events of different return intervals will be provided with the corresponding $P_f(L, I)$ maps.

4.2.1. Climate change impact for multiple rainfall events of same duration

Figure 8 shows climate change impact for 6-, 12-, and 24-hour rainfall events and provides the $P_f(L)$ maps for both present and future climate conditions. As the

proposed probabilistic framework scales the impact of intense rainfall events proportionally to the their likelihood, the events with high return intervals such as 50-, 100-year have less influence on $P_f(L)$ than more frequent rainfall events with a smaller return interval. For this reason, the change in $P_f(L)$ is not large overall for the different durations and climate conditions. However, substantial differences can be detected when the statistics are examined for different ranges of slopes. The analyses showed that the $P_f(L)$ is higher for 6-hour duration at both present and future climate conditions compared to longer duration rainfall events (Figure 8). This is attributed to the fact that the pdf values of the Gumbel distribution, $f(I | \mu, f_w, L)$ in Equation (6), for lower return interval events are higher for 6-hour duration than the corresponding values for 12- and 24-hour duration. That is, $P(F_S < 1.0 | L, I)$ in Equation (6) might be similar for different duration rainfalls as the intensity values also vary, but the $f(I | \mu, f_w, L)$ of more frequent rainfall events is higher for shorter durations.

In Figure 8, it can be seen that the $P_f(L)$ values for the future climate condition are greater than the present

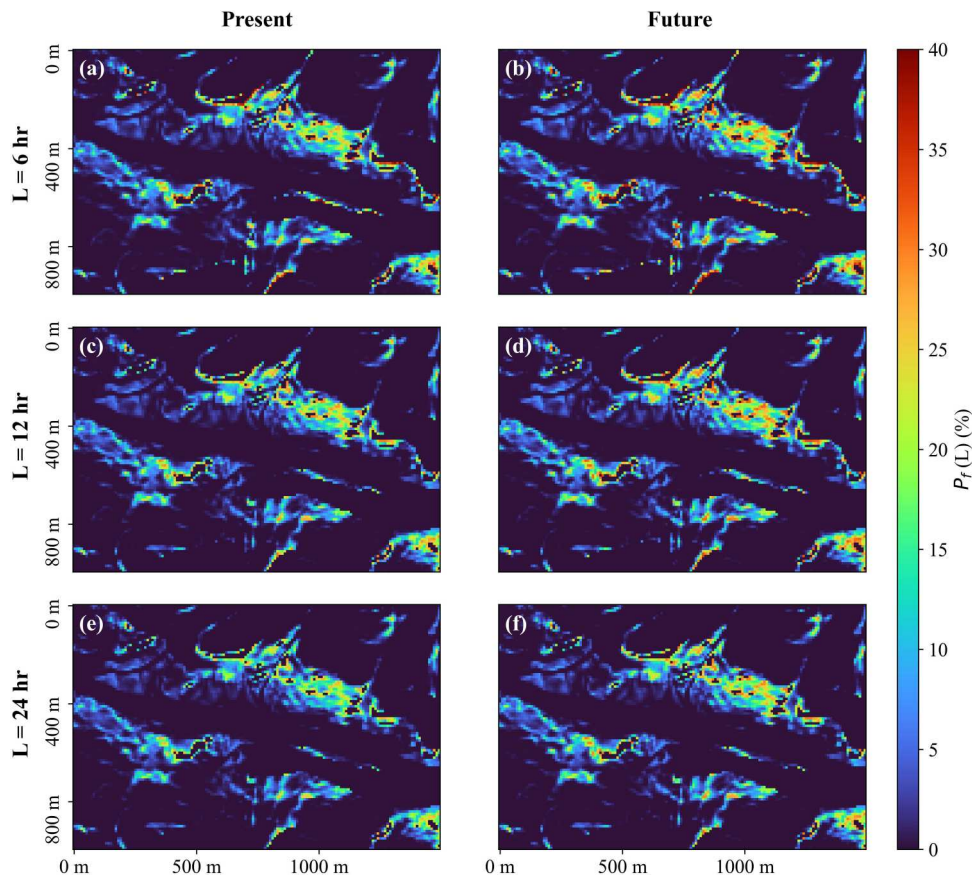


Figure 8. $P_f(L)$, maps for present (a, c, e) and future (b, d, f) climate conditions for 6-hour (a, b), 12-hour (c, d), and 24-hour (e, f) rainfall events.

condition. The difference between the $P_f(L)$ values for the present and future climate conditions (Δ) and the relative difference ($\Delta_{rel.}$) are provided in Figure 9. Additionally, mean difference ($\overline{\Delta}$), and mean relative difference ($\overline{\Delta_{rel.}}$) are tabulated in Table 2 for different ranges of slopes. It was observed that the difference, Δ , may be up to 9.7%, 8.4%, and 3.7% at certain parts of the study area for 6-, 12-, and 24-hour rainfall events, respectively. Figure 9(a–c) and Table 2 show that the $P_f(L)$ increases by approximately 3–4% over very steep slopes. Table 2 shows that the mean difference is higher for 6-hour duration for all ranges of slopes and decreases as the duration increases.

From Figure 9(d–f), and Table 2, it can be seen that there exists a relative difference of 14–20% in $P_f(L)$ for the slopes in the range 30° to 45° . Table 2 shows that $\overline{\Delta_{rel.}}$ for moderate slopes, from 25° to 30° , are very high as the small change in $P_f(L)$ at low values results in very high $\Delta_{rel.}$. Besides, in this study, the low values

of $P_f(L)$ were not estimated with high accuracy due to relatively low number of samples in Monte Carlo analysis, and therefore, these low $P_f(L)$ values have a high degree of uncertainty. It is observed that few cells have a negative difference in $P_f(L)$, which is likely due a relatively low number of samples in the Monte Carlo analysis.

Table 3 provides mean values of $P_f(L)$ for different ranges of slopes. From Table 3, it can be seen that the values of mean $P_f(L)$ are higher for 6-hour duration. As the duration increases, the mean $P_f(L)$ values decrease for each range of slopes. The effect of climate change impact on the mean $P_f(L)$ is absolute for each duration in both Tables 2 and 3. For example, the mean $P_f(L)$ increases, due to climate change, from 22.19% to 25.50%, by 3.31%, for 6-hour rainfall events over the slopes between 40° and 45° . In the literature, there exist several methods for the assessment of landslide stability in probabilistic studies, such as the

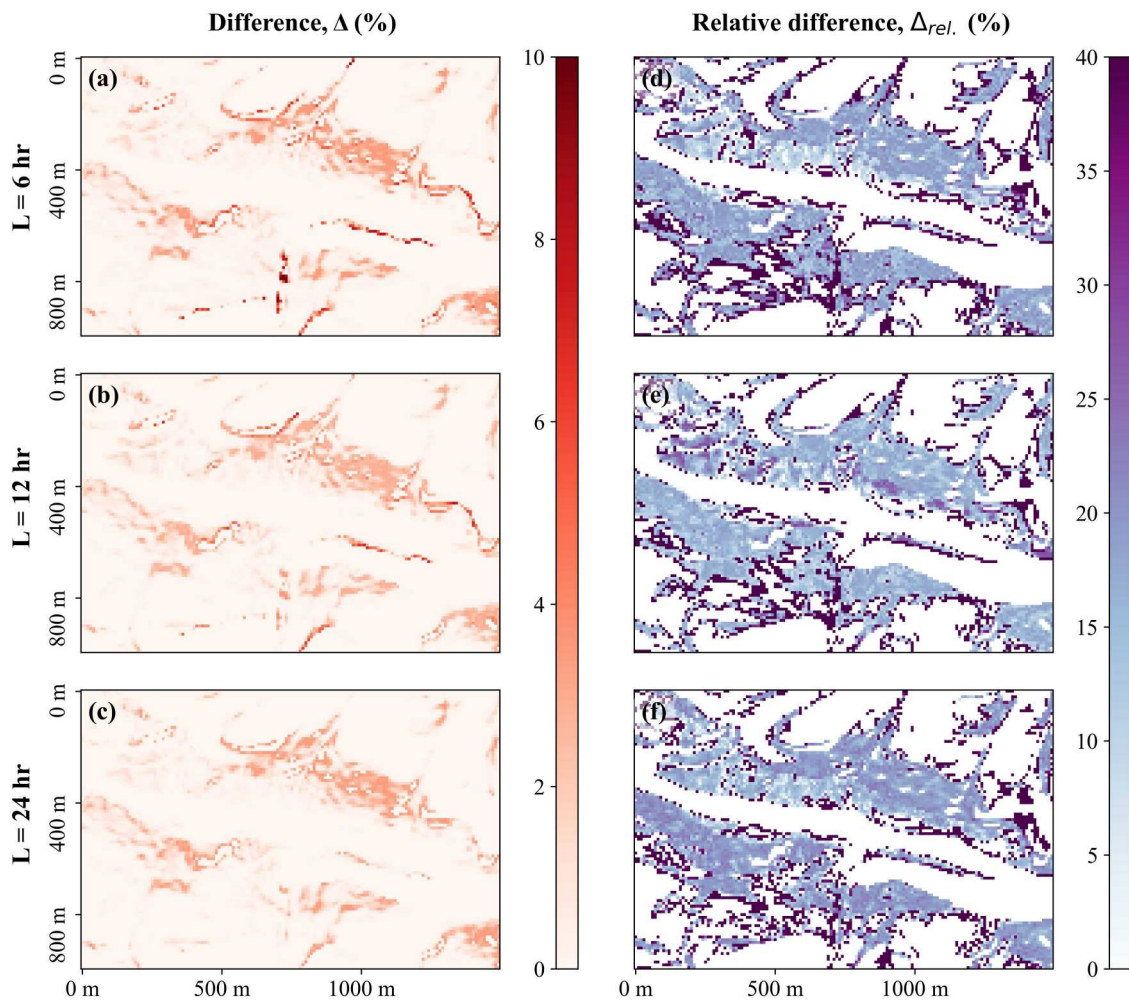


Figure 9. (a, b, c) The difference Δ between the $P_f(L)$ maps for present and future climate conditions and (d, e, f) relative difference $\Delta_{rel.}$: (a, d) 6-hour, (b, e) 12-hour, and (c, f) 24-hour.

Table 2. Mean difference $\bar{\Delta}$ and mean relative difference $\bar{\Delta}_{rel.}$ in the $P_f(L)$ over the entire area due to climate change.

Slope range °	L = 6 hr.		L = 12 hr.		L = 24 hr.	
	$\bar{\Delta}$	$\bar{\Delta}_{rel.}$	$\bar{\Delta}$	$\bar{\Delta}_{rel.}$	$\bar{\Delta}$	$\bar{\Delta}_{rel.}$
25–30	0.11	103.52	0.04	226.12	0.01	124.91
30–35	0.38	15.88	0.24	14.25	0.15	15.00
35–40	1.49	18.59	1.31	18.83	1.09	20.34
40–45	3.31	16.10	2.98	15.62	2.94	16.87

Table 3. Mean values of $P_f(L)$ for different slope ranges over the entire area.

Slope range °	L = 6 hr.		L = 12 hr.		L = 24 hr.	
	Present	Future	Present	Future	Present	Future
25–30	0.29	0.4	0.06	0.1	0.03	0.03
30–35	1.65	2.03	1.06	1.29	0.83	0.99
35–40	7.47	8.96	6.5	7.81	5.35	6.44
40–45	22.19	25.5	20.68	23.66	18.23	21.18

reliability index (Haneberg 2004), the stability index (Michel, Kobiyama, and Goerl 2014), or defining criterion on the extent with the probability of landslide initiation, P_f , greater than a certain value (Rossi et al. 2013). However, there is a lack of consensus on the assessment criteria for the susceptibility condition in the probabilistic studies. That is, there is no widely recognised level of P_f , $P_{f,limit}$ such that a slope is considered landslide-susceptible if $P_f > P_{f,limit}$ and stable otherwise. Therefore, this study employs several $P_{f,limit}$ values in the range from 10% to 40% and provides the extent of landslide-susceptible zones with a $P_f > P_{f,limit}$.

Table 4 shows the extent of zones with $P_f(L) > P_{f,limit}$ for both present and future climate conditions for 6-, 12-, and 24-hour durations. The values in parentheses are the extents of the moraine and fluvial deposits, respectively. It is observed that 6-hour duration has the larger extent regardless of $P_{f,limit}$, and has highest $P_f(L)$ values exceeding 40%. When the duration increases, the extent of zones with $P_f(L) > P_{f,limit}$ decreases. From Table 4, one can observe that climate

change significantly increases the extent of zones for each duration. It can be also seen that the extents of moraine are always greater than the extents of fluvial deposits as the moraine has larger spatial extent with steep slopes compared to the fluvial deposits.

4.2.2. Climate change impact for a given rainfall event

Landslide susceptibility simulations were performed for 6-, 12-, and 24-hour duration rainfall events of varying return intervals. The landslide susceptibility assessments were similar for different duration rainfall events of same return interval. This was attributed to having similar transient pore pressure responses for different duration rainfall events of same return interval (see Appendix A, Figure A2). In this section, the climate change impact on landslide susceptibility is provided only for 12-hour rainfall events with 10-, 50-, and 100-year return intervals for illustration purposes. The overall conclusions made for 12-hour rainfall events also applies to other durations, 6-hour and 24-hour.

Figure 10 shows the effect of climate change on the $P_f(L, I)$ values for 12-hour rainfall events with 10-, 50-, and 100-year return intervals by providing present and future conditions separately. It can be seen that the $P_f(L, I)$ values appear to be much higher in case of long return intervals, and $P_f(L, I)$ values increase due to the climate change for each return interval. The analyses showed that the increase in $P_f(L, I)$ due to climate change can be up to 22.3%, 16.9%, 13.5% at certain parts of the study area for rainfall events with 10-, 50-, and 100-year return intervals, respectively. In Table 5, the mean difference ($\bar{\Delta}$), and mean relative difference ($\bar{\Delta}_{rel.}$) in the $P_f(L, I)$ values due to climate change are provided for each return interval over different ranges of slopes. It is observed that the $\bar{\Delta}$ and $\bar{\Delta}_{rel.}$ are larger in case of 10-year return interval, and lower for 50- and 100-year return intervals. This is attributed to the fact that the steep slopes are already very close to fully saturated condition at long return intervals at the

Table 4. Extent of zones with $P_f(L) > P_{f,limit}$ over the entire area for different durations with the proportions of moraine and fluvial deposits in the parentheses.

$P_{f,limit}$ (%)	L = 6 hr.		L = 12 hr.		L = 24 hr.	
	Present	Future	Present	Future	Present	Future
10	112.85 (105.81–7.04)	131.33 (122.53–8.8)	94.7 (91.37–3.33)	114.95 (109.66–5.29)	81.98 (79.57–2.41)	97 (93.69–3.31)
20	47.68 (44.92–2.76)	65.34 (61.12–4.22)	36.63 (36.54–0.09)	49.63 (48.35–1.28)	24.21 (24.21–0)	37.38 (36.93–0.45)
30	11.63 (10.5–1.13)	23.67 (21.81–1.86)	0.76 (0.76–0)	12.38 (12.38–0)	0 (0–0)	2.44 (2.44–0)
40	2.64 (2.21–0.43)	4.08 (3.43–0.65)	0 (0–0)	0 (0–0)	0 (0–0)	0 (0–0)

Note: Unit: 10^{-2} km².

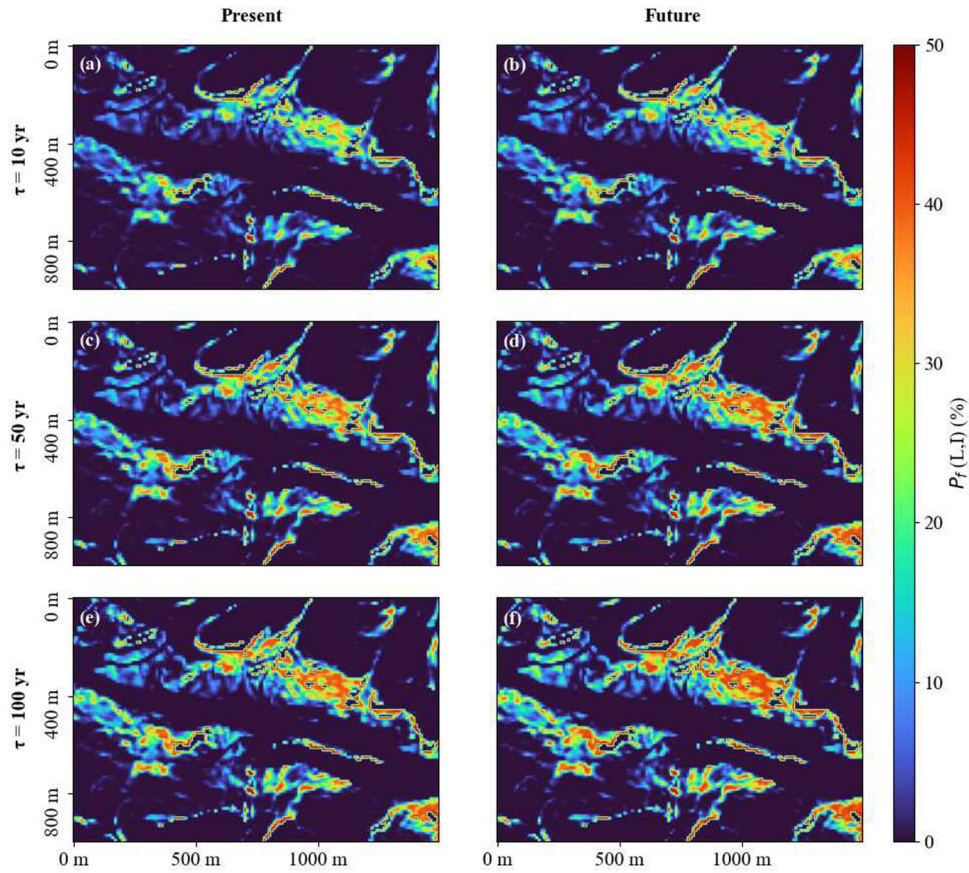


Figure 10. $P_f(L, I)$ for 12-hour rainfall events with 10-year (a, b), 50-year (c, d), and 100-year (e, f) return intervals for present (a, c, e) and future (b, d, f) climate conditions.

present condition. Larger precipitation can just make the slope fully saturated, resulting in considerably less change in $P_f(L, I)$ values.

The mean values of $P_f(L, I)$ over different ranges of slopes are provided in Table 6 for each return interval. It can be seen that the mean $P_f(L, I)$ increases as the return interval increases, for each slope range. Table 6 reveals that the climate change increases the mean $P_f(L, I)$ and results in more susceptible slopes for all slope ranges. From both Tables 5 and 6, it can be seen that the change in mean $P_f(L, I)$ is higher for 10-year return interval events. However, the mean $P_f(L, I)$

values reach the highest value for 100-year return interval events. Additionally, it is observed the $P_f(L, I)$ values over a slope range may have a very wide range. That is, two identical slopes might have different $P_f(L, I)$ values. This is attributed, among others, to the observation that the excess rainfall due to fully saturation is redistributed to the surrounding neighbouring regions. Therefore, a slope might receive more water than another slope with the same inclination. Table 7 shows the extent of zones with $P_f(L, I) > P_{f,limit}$ for both present and future climate conditions for 12-hour rainfall events of 10-, 50-, and 100-year return intervals. The extents of moraine and fluvial deposits are provided in the parentheses. From Table 7, it is observed that the extent of susceptible zones increases as the return interval increases and 100-year return interval has the largest extent regardless of $P_{f,limit}$. The impact of climate change on the extent of zones can be clearly seen in Table 7. For example, climate change increases the extent of zones with $P_f(L, I) > 40\%$ by a factor of 1.5 – 2.7 depending on the return interval.

Table 5. Mean difference $\bar{\Delta}$ and mean relative difference $\bar{\Delta}_{rel.}$ in $P_f(L, I)$ for 12-hour rainfall events over the entire area due to climate change.

Slope range °	$\tau = 10$ yr.		$\tau = 50$ yr.		$\tau = 100$ yr.	
	$\bar{\Delta}$	$\bar{\Delta}_{rel.}$	$\bar{\Delta}$	$\bar{\Delta}_{rel.}$	$\bar{\Delta}$	$\bar{\Delta}_{rel.}$
25–30	0.15	176.68	0.12	31.66	0.13	28.08
30–35	0.69	47.80	0.47	22.02	0.80	17.13
35–40	3.02	31.78	2.04	17.54	2.98	19.89
40–45	4.57	17.74	1.96	6.03	1.36	4.07

Table 6. Mean values of $P_f(L, I)$ for 12-hour rainfall events for different slope ranges over the entire area.

Slope range °	$\tau = 10$ yr.		$\tau = 50$ yr.		$\tau = 100$ yr.	
	Present	Future	Present	Future	Present	Future
25–30	0.16	0.31	0.52	0.64	0.62	0.76
30–35	1.44	2.13	3.39	3.86	3.77	4.57
35–40	9.77	12.79	16.86	18.89	18.51	21.49
40–45	28.74	33.31	36.87	38.84	38.67	40.02

Table 7. Extent of zones with $P_f(L, I) > P_{f,limit}$ over the entire area for 12-hour rainfall events of different return intervals with the proportions of moraine and fluvial deposits in the parentheses.

$P_{f,limit}$ (%)	$\tau = 10$ yr.		$\tau = 50$ yr.		$\tau = 100$ yr.	
	Present	Future	Present	Future	Present	Future
10	136.98 (128.91–8.07)	162.69 (150.52–12.17)	195.92 (179.42–16.5)	213.87 (195.91–17.96)	211.35 (193.96–17.39)	246.75 (224.73–22.02)
20	73.61 (69.72–3.89)	97.65 (91.82–5.83)	132.26 (123.77–8.49)	141.78 (131.51–10.27)	140.45 (130.57–9.88)	161.91 (149.87–12.04)
30	35.3 (33.67–1.63)	58.73 (55.57–3.16)	86.47 (81.32–5.15)	99.27 (92.66–6.61)	98.59 (92.12–6.47)	115.71 (108.18–7.53)
40	5.18 (4.47–0.71)	14.00 (12.53–1.47)	24.39 (21.54–2.85)	37.14 (33.72–3.42)	33.59 (30.21–3.38)	53.67 (49.7–3.97)

Note: Unit: 10^{-2} km².

5. Overall discussion

This study proposed a novel implementation of probabilistic framework to quantify the impact of climate change on landslide susceptibility by accounting for multiple rainfall events. The framework accounts for both the uncertainties in landslide and climate models by Monte Carlo method. The probabilistic framework, Equation (6), combines the results from the climate and landslide models by integrating the landslide susceptibility estimates over different intensity values with varying return intervals for a given duration. By doing so, the contributions of rainfall events to the climate change impact were scaled with respect to their probability of occurrence. Otherwise, climate change impact on landslide susceptibility would likely be overestimated by using only extreme rainfall events with long return intervals despite their low occurrence probability (see Section 4.2).

The proposed framework mitigates bias in climate change impact studies resulting from less likely high intense rainfall events and provides more robust and reliable predictions. This framework leads to accurate quantification of climate change impact and detection of critical zones with a higher increase in the probability of landslide initiation under climate change. As a result, it offers valuable insights and provides a basis to mitigate the upcoming landslide risk and strengthen the resilience and adaptive capacity of society under climate change. Moreover, such analyses can be of great advantage in engineering practice by better identifying landslide-susceptible areas in the light of changing climate,

supporting areal planning, and facilitating infrastructure development.

This study quantified the climate change impact for 6-, 12-, and 24-hour rainfall events by the proposed probabilistic framework (Section 2.3) and provided $P_f(L)$ maps for present and future climate conditions (Figure 8). The increase in $P_f(L)$ due to climate change can be up to 9.7%, 8.4%, and 3.7% for 6-, 12-, and 24-hour rainfall events, respectively (Figure 9). For both moraine and fluvial deposits, a considerable increase in the extent of susceptible zones based on different values of $P_{f,limit}$ (Table 4) was observed. In addition, climate change impact was also illustrated by 12-hour rainfall events of 10-, 50-, and 100-year return intervals (Figure 10). This may be particularly important for engineering structures such as infrastructures, buildings, or any other project designed based on extreme rainfall events. The study revealed that climate change increases both $P_f(L, I)$ (Tables 5 and 6) and the extent of susceptible zones (Table 7). For 12-hour rainfall events of 10-, 50-, and 100-year return intervals, the increase in $P_f(L, I)$ due to climate change can be up to 22.3%, 16.9%, and 13.5%, respectively. The results of this study also showed that the moraine soil type poses a higher risk than the fluvial deposits under the climate change (Tables 4 and 7). This is due to the moraine being more located on steep slopes than fluvial deposits.

There are many sources of uncertainty in the climate modelling chain, such as biases in RCMs and the driving GCMs, assumptions about future emissions, the limited

size of the model ensemble, uncertainties associated with precipitation observations, and the approximate formula used to calculate IDF curves (Equation (1)). When it comes to uncertainties associated with climate models, previous model evaluation done in connection to statistical downscaling has indicated that GCMs are able to reproduce the large-scale conditions found in nature that are important to local climate variations (Benestad 2021).

The current study included only the high emission scenario RCP8.5, which is based on the assumptions of no climate policy, high population growth and slow technological development, resulting in continued increases of greenhouse gases throughout the twenty-first century. The results presented here can therefore be interpreted as high-end estimates of change. Other scenarios based on assumptions of decreased emissions show smaller changes in the precipitation and thus would have given a smaller change in the landslide susceptibility. Similarly, the projected landslide susceptibility was provided only for the end of the century (2071–2100). Projections of landslide susceptibility to the near future (2021–2050) were also performed. The results showed smaller increase in the probability of landslide initiation over the entire area compared to the values at the end of the century (2071–2100).

This study is promising in the way forward to quantification of the climate change impact by accounting for the likelihood of rainfall events. Due to the complexities in both landslide and climate modelling chains, there exist several shortcomings that should be addressed in future studies for a more complete and comprehensive landslide susceptibility assessments. The shortcomings can be listed as follows:

- In the landslide susceptibility analyses, the complex geological and environmental processes, snowmelt-ing, vegetation, and areal planning were not accounted for due to the limitations of the physical-based model and the high level of complexities involved. It should be noted that these processes, such climate driven changes in natural disturbance (Scheidl et al. 2020) or snow melting may significantly affect the landslide susceptibility. The current study provided only a partial view of climate change impact on landslide susceptibility, lacking of the contribution of these complex processes.
- Calibration of the landslide susceptibility model is based on a conventional deterministic approach with an objective junction, and several assumptions were made due to the lack of information on soil parameters, initial conditions, and incomplete landslide inventory. More advanced probabilistic calibration

methods accounting for spatial variable model parameters (e.g. Depina, Oguz, and Thakur 2020; Luo et al. 2022) can be also utilised depending on the availability of information on soil parameters, and completeness of landslide inventory. Different calibration strategies could lead to different parameter sets, leading to different levels of increase in $P_f(L)$ and $P_f(L, I)$ due to climate change.

- Due to the insufficient knowledge on the hydrological conditions and the lack of laboratory and field test, the hydrological parameters, K_S and D_0 were determined by conducting a parametric hydrological analysis (Appendix A) and by considering the values reported in the literature. Effects of varying K_S and D_0 on the probability of landslide initiation have been investigated. Overall findings of the current study only differ only when hydraulic parameters result in extremely slow or fast infiltration.
- It should be noted that this study did not account for the spatial variability of the geotechnical and hydrological model parameters, which may show strong variability through space (e.g. Jiang et al. 2022; Lei et al. 2023; Oguz, Depina, and Thakur 2022). Instead, these parameters were assumed homogeneous within a single geological unit and the variability of the model parameters has been modelled with a single random variable approach using the Monte Carlo method.
- The Euro-CORDEX ensemble is relatively small in terms of providing robust values for the future and the small sample size may lead to an unrepresentative, narrow and skewed view of the range of possible outcomes of climate change (Mezghani et al. 2019). Ideally, future regional projections should include empirical-statistical downscaling or hybrid downscaling as well as RCM results to enable including a larger ensemble of GCMs and thus provide more entrusted results (Benestad 2021). However, empirical-statistical downscaling of precipitation and in particular the precipitation intensity is challenging due to the large local and stochastic variations. Research is nevertheless ongoing with the aim to find good ESD-based and hybrid downscaling solutions for precipitation statistics.
- This study estimated the local effects of climate change based on dynamically downscaled data that had not been bias-corrected. To address potential issues related to biases, we opted for a delta change approach (e.g. Hay, Wilby, and Leavesley 2000), where the present conditions were represented by observations and future conditions were estimated by adding the change from RCM simulations. While bias correction might have given a more physically consistent picture of the

precipitation climate of the future, fewer bias corrected RCM simulations were available, and in the context of this study we considered the benefit of a larger ensemble of climate model simulations greater than the potential advantage of bias correction.

- In this study, climate-dependent IDF curves were developed only for one weather station, which was found to be reliable with long observation data. Therefore, rainfall events were modelled as constant over the entire area in the TRIGRS model. Accounting spatial variability of the precipitation may affect the landslide susceptibility (e.g. Shou and Yang 2015) and more realistic results could be obtained.

6. Summary

The changes in the rainfall patterns are commonly known to a certain degree for different spatial and temporal scales. However, the effect of these changes on landslide susceptibility was rarely quantified explicitly. Such quantification will provide a basis for the development of mitigation strategies for landslide risk under climate change. This study presented a framework for the quantification of climate change impact on rainfall-induced landslide susceptibility. The framework consists of climate and landslide modelling chains. One of the novelties of the study comes from incorporating a simple semi-empirical formulation to estimate the approximate daily and sub-daily rainfall statistics, and utilising these statistics in the landslide modelling chain. Additional novelties include the implementation of a probabilistic framework to integrate the two modelling chains and obtain the climate change impact by accounting for multiple rainfall events of the same duration, instead of only investigating extreme rainfall events. The proposed probabilistic framework accounts for the likelihood of rainfall events for a given duration rainfall and scales the contributions of these intense rainfall events by their probability of occurrences.

The current study quantified the climate change impact on rainfall-induced shallow landslide susceptibility for a landslide-prone region located in central Norway. The climate change impact was quantified for varying duration rainfall events with the proposed probabilistic framework. Additionally, the impact was also quantified for extreme rainfall events of long return intervals. The results demonstrated that the landslide susceptibility over the study area increases due to climate change with higher probabilities of landslide initiation, and larger landslide-susceptible extents. The proposed probabilistic framework provided a more realistic basis

for the evaluation of the climate change impact on landslide susceptibility without the bias due to extreme rainfall events with low probability of occurrence.

Acknowledgments

The authors are grateful to Dr. Graziella Devoli from the Norwegian Water Resources and Energy Directorate for her support on the interpretation of the geology and the landslide inventory. The authors extend their gratitude to the partners involved in the R&D project KlimaDigital (2018-2022, grant number: 281059), including SINTEF, Norwegian University of Science and Technology (NTNU), Norwegian Meteorological Institute (MET), Geonor, Nordic Semiconductor, Telia, Norwegian Public Roads Administration, and Norwegian Water Resources and Energy Directorate (NVE).

Disclosure statement

No potential conflict of interest was reported by the authors.

Funding

The authors acknowledge support from the R&D project KlimaDigital (2018–2022, grant number 281059) that is funded by the Research Council of Norway (Norges Forskningsrød) and by SINTEF, Norwegian University of Science and Technology (NTNU), Norwegian Meteorological Institute (MET), Geonor, Nordic Semiconductor, Telia, Norwegian Public Roads Administration, and Norwegian Water Resources and Energy Directorate (NVE). The authors also acknowledge support through the project KK.01.1.1.02.0027 that is financed by the Croatian Government and the European Union through the Regional Development Fund – the Competitiveness and Cohesion Operational Programme.

ORCID

Emir Ahmet Oguz  <http://orcid.org/0000-0002-1158-1926>

References

- Alvioli, M., and R. L. Baum. 2016. “Parallelization of the TRIGRS Model for Rainfall-Induced Landslides Using the Message Passing Interface.” *Environmental Modelling and Software* 81:122–135. <https://doi.org/10.1016/j.envsoft.2016.04.002>.
- Alvioli, M., M. Melillo, F. Guzzetti, M. Rossi, E. Palazzi, J. von Hardenberg, M. T. Brunetti, and S. Peruccacci. 2018. “Implications of Climate Change on Landslide Hazard in Central Italy.” *Science of the Total Environment* 630:1528–1543. <https://doi.org/10.1016/j.scitotenv.2018.02.315>.
- Arnone, E., Y. G. Dialynas, L. V. Noto, and R. L. Bras. 2016. “Accounting for Soil Parameter Uncertainty in a Physically Based and Distributed Approach for Rainfall-Triggered Landslides.” *Hydrological Processes* 30 (6): 927–944. <https://doi.org/10.1002/hyp.10609>.

- Baecher, G. B., and J. T. Christian. 2003. *Reliability and Statistics in Geotechnical Engineering*. West Sussex, England: John Wiley & Sons.
- Barik, M. G., J. C. Adam, M. E. Barber, and B. Muhunthan. 2017. "Improved Landslide Susceptibility Prediction for Sustainable Forest Management in an Altered Climate." *Engineering Geology* 230:104–117. <https://doi.org/10.1016/j.enggeo.2017.09.026>.
- Baum, R. L., J. W. Godt, and W. Z. Savage. 2010. "Estimating the Timing and Location of Shallow Rainfall-Induced Landslides Using a Model for Transient, Unsaturated Infiltration." *Journal of Geophysical Research: Earth Surface* 115. <https://doi.org/10.1029/2009JF001321>.
- Baum, B. R. L., W. Z. Savage, and J. W. Godt. 2002. "TRIGRS – a Fortran Program for Transient Rainfall Infiltration and Grid-Based Regional Slope-Stability Analysis: Open-File Report 02-424." Technical Report USGS.
- Baum, R. L., W. Z. Savage, and J. W. Godt. 2008. "TRIGRS – a Fortran Program for Transient Rainfall Infiltration and Grid-Based Regional Slope-Stability Analysis, Version 2.0: U.S. Geological Survey Open-File Report, 2008-1159. Technical Report U.S. Geological Survey.
- Beldring, S., K. Engeland, L. A. Roald, N. R. Sælthun, and A. Vokso. 2003. "Estimation of Parameters in a Distributed Precipitation-Runoff Model for Norway." *Hydrology and Earth System Sciences* 7 (3): 304–316. <https://doi.org/10.5194/hess-7-304-2003>.
- Benestad, R. E. 2021. "A Norwegian Approach to Downscaling." Technical Report Climate and Earth System Modeling. <https://doi.org/10.5194/gmd-2021-176>.
- Benestad, R. E., J. Lutz, A. V. Dyrddal, J. E. Haugen, K. M. Parding, and A. Dobler. 2021. "Testing a Simple Formula for Calculating Approximate Intensity-Duration-Frequency Curves." *Environmental Research Letters* 16 (4): 044009. <https://doi.org/10.1088/1748-9326/abd4ab>.
- Benestad, R. E., K. M. Parding, H. B. Erlandsen, and A. Mezghani. 2019. "A Simple Equation to Study Changes in Rainfall Statistics." *Environmental Research Letters* 14 (8): 084017. <https://doi.org/10.1088/1748-9326/ab2bb2>.
- Benestad, R. E., K. M. Parding, K. Isaksen, and A. Mezghani. 2016. "Climate Change and Projections for the Barents Region: What is Expected to Change and What Will Stay the Same?" *Environmental Research Letters* 11 (5): 054017. <https://doi.org/10.1088/1748-9326/11/5/054017>.
- Benestad, R., K. Parding, A. Mezghani, A. Dobler, O. Landgren, H. Erlandsen, J. Lutz, and J. Haugen. 2019. "Stress Testing for Climate Impacts with 'Synthetic Storms'." *Eos Transactions American Geophysical Union* 100 100. <https://doi.org/10.1029/2019eo113311>.
- Chang, Z., Z. Du, F. Zhang, F. Huang, J. Chen, W. Li, and Z. Guo. 2020. "Landslide Susceptibility Prediction Based on Remote Sensing Images and GIS: Comparisons of Supervised and Unsupervised Machine Learning Models." *Remote Sensing* 12. <https://doi.org/10.3390/rs12030502>.
- Chiang, S. H., and K. T. Chang. 2011. "The Potential Impact of Climate Change on Typhoon-Triggered Landslides in Taiwan, 2010–2099." *Geomorphology* 133 (3-4): 143–151. <https://doi.org/10.1016/j.geomorph.2010.12.028>.
- Ciervo, F., G. Rianna, P. Mercogliano, and M. N. Papa. 2017. "Effects of Climate Change on Shallow Landslides in a Small Coastal Catchment in Southern Italy." *Landslides* 14 (3): 1043–1055. <https://doi.org/10.1007/s10346-016-0743-1>.
- Ciurleo, M., M. C. Mandaglio, and N. Moraci. 2019. "Landslide Susceptibility Assessment by TRIGRS in a Frequently Affected Shallow Instability Area." *Landslides* 16 (1): 175–188. <https://doi.org/10.1007/s10346-018-1072-3>.
- Comegna, L., L. Picarelli, E. Bucchignani, and P. Mercogliano. 2013. "Potential Effects of Incoming Climate Changes on the Behaviour of Slow Active Landslides in Clay." *Landslides* 10 (4): 373–391. <https://doi.org/10.1007/s10346-012-0339-3>.
- Dehn, M., G. Bürger, J. Buma, and P. Gasparetto. 2000. "Impact of Climate Change on Slope Stability Using Expanded Downscaling." *Engineering Geology* 55 (3): 193–204. [https://doi.org/10.1016/S0013-7952\(99\)00123-4](https://doi.org/10.1016/S0013-7952(99)00123-4).
- Depina, I., E. A. Oguz, and V. Thakur. 2020. "Novel Bayesian Framework for Calibration of Spatially Distributed Physical-Based Landslide Prediction Models." *Computers and Geotechnics* 125:103660. <https://doi.org/10.1016/j.compgeo.2020.103660>.
- Devoli, G., R. Bell, and J. Cepeda. 2019. "NVE Report 1/2019: Susceptibility Map at Catchment Level, to be Used in Landslide Forecasting, Norway. Technical Report 1 NVE Oslo, Norway.
- Dixon, N., and E. Brook. 2007. "Impact of Predicted Climate Change on Landslide Reactivation: Case Study of Mam Tor, UK." *Landslides* 4 (2): 137–147. <https://doi.org/10.1007/s10346-006-0071-y>.
- Dyrddal, A. V., and E. J. Førland. 2019. "Klimapåslag for Korttidsnedbør: Anbefalte Verdier for Norge." Technical Report 5/2019.
- Erlandsen, H. B., K. M. Parding, R. Benestad, A. Mezghani, and M. Pontoppidan. 2020. "A Hybrid Downscaling Approach for Future Temperature and Precipitation Change." *Journal of Applied Meteorology and Climatology* 59 (11): 1793–1807. <https://doi.org/10.1175/JAMC-D-20-0013.1>.
- Eyring, V., S. Bony, G. A. Meehl, C. A. Senior, B. Stevens, R. J. Stouffer, and K. E. Taylor. 2016. "Overview of the Coupled Model Intercomparison Project Phase 6 (CMIP6) Experimental Design and Organization." *Geoscientific Model Development* 9 (5): 1937–1958. <https://doi.org/10.5194/gmd-9-1937-2016>.
- Fawcett, T. 2006. "An Introduction to ROC Analysis." *Pattern Recognition Letters* 27 (8): 861–874. <https://doi.org/10.1016/j.patrec.2005.10.010>.
- Fenton, G. A., and D. V. Griffiths. 2008. *Risk Assessment in Geotechnical Engineering*. New Jersey: United States: John Wiley & Sons. DOI:10.1002/9780470284704.
- Fischer, L., L. Rubensdotter, K. Sletten, K. Stalsberg, C. Melchiorre, P. Horton, and M. Jaboyedoff. 2012. "Debris Flow Modeling for Susceptibility Mapping at Regional to National Scale in Norway." In *Landslides and Engineered Slopes: Protecting Society Through Improved Understanding – Proceedings of the 11th International and 2nd North American Symposium on Landslides and Engineered Slopes, 2012*, 723–729.
- Gariano, S. L., and F. Guzzetti. 2016. "Landslides in a Changing Climate." *Earth-Science Reviews* 162:227–252. <https://doi.org/10.1016/j.earscirev.2016.08.011>.
- Haneberg, W. C. 2004. "A Rational Probabilistic Method for Spatially Distributed Landslide Hazard Assessment." *Environmental and Engineering Geoscience* 10 (1): 27–43. <https://doi.org/10.2113/10.1.27>.

- Hanssen-Bauer, I., E. J. Førland, I. Haddeland, H. Hisdal, D. Lawrence, S. Mayer, A. Nesje, et al. 2017. "Climate in Norway 2100 – a Knowledge Base for Climate Adaptation." Technical Report 1. www.miljodirektoratet.no/M741.
- Hay, L. E., R. L. Wilby, and G. H. Leavesley. 2000. "A Comparison of Delta Change and Downscaled GCM Scenarios for Three Mountain Basins in the United States." *Journal Of The American Water Resources Association* 36 (2): 387–397. <https://doi.org/10.1111/j.1752-1688.2000.tb04276.x>.
- Ho, K., S. Lacasse, and L. Picarelli. 2017. *Slope Safety Preparedness for Impact of Climate Change*. 1st ed., 10.1201/9781315387789.
- Hu, W., A. S. Ming, J. W. Quan, J. Fan, and K Reichardt. 2008. "Spatial Variability of Soil Hydraulic Properties on a Steep Slope in the Loess Plateau of China." *Scientia Agricola* 65 (3): 268–276. <https://doi.org/10.1590/S0103-90162008000300007>.
- Huang, F., Z. Cao, J. Guo, S. H. Jiang, S. Li, and Z Guo. 2020. "Comparisons of Heuristic, General Statistical and Machine Learning Models for Landslide Susceptibility Prediction and Mapping." *Catena* 191:104580. <https://doi.org/10.1016/j.catena.2020.104580>.
- Huang, F., Z. Cao, S. H. Jiang, C. Zhou, J. Huang, and Z Guo. 2020. "Landslide Susceptibility Prediction Based on a Semi-Supervised Multiple-Layer Perceptron Model." *Landslides* 17 (12): 2919–2930. <https://doi.org/10.1007/s10346-020-01473-9>.
- Huang, J. C., and S. J. Kao. 2006. "Optimal Estimator for Assessing Landslide Model Performance." *Hydrology and Earth System Sciences* 10 (6): 957–965. <https://doi.org/10.5194/hess-10-957-2006>.
- Huang, F., J. Zhang, C. Zhou, Y. Wang, J. Huang, and L. Zhu. 2020. "A Deep Learning Algorithm Using a Fully Connected Sparse Autoencoder Neural Network for Landslide Susceptibility Prediction." *Landslides* 17 (1): 217–229. <https://doi.org/10.1007/s10346-019-01274-9>.
- IPCC. 2012. "Managing the Risks of Extreme Events and Disasters to Advance Climate Change Adaptation." A Special Report of Working Groups I and II of the Intergovernmental Panel on Climate Change. Cambridge, UK, and New York, NY, USA: Cambridge University Press.
- IPCC. 2014. "Climate Change 2014: Synthesis Report." Technical Report IPCC Geneva, Switzerland.
- IPCC. 2021. "Climate Change 2021: The Physical Science Basis." Contribution of Working Group I to the Sixth Assessment Report of the Intergovernmental Panel on Climate Change. Technical Report 3-.
- Iverson, R. M. 2000. "Landslide Triggering by Rain Infiltration." *Water Resources Research* 36 (7): 1897–1910. <https://doi.org/10.1029/2000WR900090>.
- Jacob, D., J. Petersen, B. Eggert, A. Alias, O. B. Christensen, L. M. Bouwer, A. Braun, et al. 2014. "EURO-CORDEX: New High-Resolution Climate Change Projections for European Impact Research." *Regional Environmental Change* 14 (2): 563–578. <https://doi.org/10.1007/s10113-013-0499-2>.
- Javankhoshdel, S., and R. J Bathurst. 2016. "Influence of Cross Correlation between Soil Parameters on Probability of Failure of Simple Cohesive and C- ϕ Slopes." *Canadian Geotechnical Journal* 53 (5): 839–853. <https://doi.org/10.1139/cgj-2015-0109>.
- Jiang, S. H., J. Huang, D. V. Griffiths, and Z. P. Deng. 2022. "Advances in Reliability and Risk Analyses of Slopes in Spatially Variable Soils: A State-of-the-Art Review." *Computers and Geotechnics* 141:104498. <https://doi.org/10.1016/j.compgeo.2021.104498>.
- Kainthura, P., and N Sharma. 2022. "Machine Learning Driven Landslide Susceptibility Prediction for the Uttarkashi Region of Uttarakhand in India." *Georisk* 16:570–583. <https://doi.org/10.1080/17499518.2021.1957484>.
- Kartverket. n.d. "Høydedata." Date accessed March 18, 2023.
- Lacasse, S., F. Nadim, and B Kalsnes. 2010. "Living with Landslide Risk." *Geotechnical Engineering Journal of the SEAGS & AGSSEA* 41. <https://www.engmath.dal.ca/tc32/>.
- Lei, Y., J. Huang, Y. Cui, S. H. Jiang, S. Wu, and J Ching. 2023. "Time Capsule for Landslide Risk Assessment." *Georisk*. <https://doi.org/10.1080/17499518.2023.2164899>.
- Liu, C. N., and C. C Wu. 2008. "Mapping Susceptibility of Rainfall-Triggered Shallow Landslides Using a Probabilistic Approach." *Environmental Geology* 55 (4): 907–915. <https://doi.org/10.1007/s00254-007-1042-x>.
- Luo, J., L. Zhang, H. Yang, X. Wei, D. Liu, and J Xu. 2022. "Probabilistic Model Calibration of Spatial Variability for a Physically-Based Landslide Susceptibility Model." *Georisk* 16:728–745. <https://doi.org/10.1080/17499518.2021.1988986>.
- Melchiorre, C., and P Frattini. 2012. "Modelling Probability of Rainfall-Induced Shallow Landslides in a Changing Climate, Otta, Central Norway." *Climatic Change* 113 (2): 413–436. <https://doi.org/10.1007/s10584-011-0325-0>.
- Mergili, M., I. Marchesini, M. Rossi, F. Guzzetti, and W Fellin. 2014. "Spatially Distributed Three-Dimensional Slope Stability Modelling in a Raster GIS." *Geomorphology* 206:178–195. <https://doi.org/10.1016/j.geomorph.2013.10.008>.
- MET. n.d. "What is Frost?" Date accessed March 18, 2023.
- Mezghani, A., A. Dobler, R. Benestad, J. E. Haugen, K. M. Parding, M. Piniewski, and Z. W Kundzewicz. 2019. "Subsampling Impact on the Climate Change Signal Over Poland Based on Simulations from Statistical and Dynamical Downscaling." *Journal of Applied Meteorology and Climatology* 58 (5): 1061–1078. <https://doi.org/10.1175/JAMC-D-18-0179.1>.
- Michel, G. P., M. Kobiyama, and R. F Goerl. 2014. "Comparative Analysis of SHALSTAB and SINMAP for Landslide Susceptibility Mapping in the Cunha River Basin, Southern Brazil." *Journal of Soils and Sediments* 14 (7): 1266–1277. <https://doi.org/10.1007/s11368-014-0886-4>.
- Montgomery, D. R., and W. E Dietrich. 1994. "A Physically Based Model for the Topographic Control on Shallow Landsliding." *Water Resources Research* 30 (4): 1153–1171. <https://doi.org/10.1029/93WR02979>.
- Montrasio, L., and R Valentino. 2008. "A Model for Triggering Mechanisms of Shallow Landslides." *Natural Hazards and Earth System Science* 8 (5): 1149–1159. <https://doi.org/10.5194/nhess-8-1149-2008>.
- Mtongori, H. I., F. Stordal, R. E. Benestad, S. K. Mourice, F. Justino, C. Kikuu, A. Meteorology, and P Agricultural. 2015. "Impacts of Climate and Farming Management on Maize Yield in SouthernTanzania." *African Crop Science Journal* 23 (4): 399–417. <https://doi.org/10.4314/acsj.v23i4.9>.

- NGU. n.d. "Datasets." Date accessed March 18, 2023.
- NVE. n.d. "Skredregistrering." Date accessed March 18, 2023.
- Oguz, E. A., I. Depina, B. Myhre, G. Devoli, H. Rustad, and V Thakur. 2022. "IoT-Based Hydrological Monitoring of Water-Induced Landslides: A Case Study in Central Norway." *Bulletin of Engineering Geology and the Environment* 81 (5). <https://doi.org/10.1007/s10064-022-02721-z>.
- Oguz, E. A., I. Depina, and V Thakur. 2022. "Effects of Soil Heterogeneity on Susceptibility of Shallow Landslides." *Landslides* 19 (1): 67–83. <https://doi.org/10.1007/s10346-021-01738-x>.
- Pack, R., D. Tarboton, C. Goodwin, and A. Prasad. 2005. "SINMAP 2.0: A Stability Index Approach to Terrain Stability Hazard Mapping."
- Park, D. W., N. V. Nikhil, and S. R. Lee. 2013. "Landslide and Debris Flow Susceptibility Zonation Using TRIGRS for the 2011 Seoul Landslide Event." *Natural Hazards and Earth System Science*, 2833–2849. <https://doi.org/10.5194/nhess-13-2833-2013>.
- Pecoraro, G., M. Calvello, and L Piciullo. 2019. "Monitoring Strategies for Local Landslide Early Warning Systems." *Landslides* 16 (2): 213–231. <https://doi.org/10.1007/s10346-018-1068-z>.
- Phoon, K. K., and F. H Kulhawy. 1999. "Characterization of Geotechnical Variability." *Canadian Geotechnical Journal* 36 (4): 612–624. <https://doi.org/10.1139/t99-038>.
- Raia, S., M. Alvioli, M. Rossi, R. L. Baum, J. W. Godt, and F Guzzetti. 2014. "Improving Predictive Power of Physically Based Rainfall-Induced Shallow Landslide Models: A Probabilistic Approach." *Geoscientific Model Development* 7 (2): 495–514. <https://doi.org/10.5194/gmd-7-495-2014>.
- Rianna, G., A. Zollo, P. Tommasi, M. Paciucci, L. Comegna, and P Mercogliano. 2014. "Evaluation of the Effects of Climate Changes on Landslide Activity of Orvieto Clayey Slope." *Procedia Earth and Planetary Science* 9:54–63. <https://doi.org/10.1016/j.proeps.2014.06.017>.
- Rossi, G., F. Catani, L. Leoni, S. Segoni, and V Tofani. 2013. "HIRESSS: A Physically Based Slope Stability Simulator for HPC Applications." *Natural Hazards and Earth System Science* 13 (1): 151–166. <https://doi.org/10.5194/nhess-13-151-2013>.
- Salciarini, D., L. Brocca, S. Camici, L. Ciabatta, E. Volpe, R. Massini, and C Tamagnini. 2019. "Physically Based Approach for Rainfall-Induced Landslide Projections in a Changing Climate." *Proceedings of the Institution of Civil Engineers: Geotechnical Engineering* 172 (6): 481–495. <https://doi.org/10.1680/jgeen.18.00216>.
- Sangelantoni, L., E. Gioia, and F Marincioni. 2018. "Impact of Climate Change on Landslides Frequency: The Esino River Basin Case Study (Central Italy)." *Natural Hazards* 93 (2): 849–884. Springer Netherlands. <https://doi.org/10.1007/s11069-018-3328-6>.
- Scheidl, C., M. Heiser, S. Kamper, T. Thaler, K. Klebinder, F. Nagl, V. Lechner, et al. 2020. "The Influence of Climate Change and Canopy Disturbances on Landslide Susceptibility in Headwater Catchments." *Science of the Total Environment* 742:140588. <https://doi.org/10.1016/j.scitotenv.2020.140588>.
- Shou, K. J., and C. M Yang. 2015. "Predictive Analysis of Landslide Susceptibility under Climate Change Conditions – a Study on the Chingshui River Watershed of Taiwan." *Engineering Geology* 192:46–62. <https://doi.org/10.1016/j.enggeo.2015.03.012>.
- Simoni, S., F. Zanotti, G. Bertoldi, and R Rigon. 2008. "Modelling the Probability of Occurrence of Shallow Landslides and Channelized Debris Flows Using GEOtop-FS." *Hydrological Processes* 22 (4): 532–545. <https://doi.org/10.1002/hyp.6886Modelling>.
- Su, C., B. Wang, Y. Lv, M. Zhang, D. Peng, B. Bate, and S Zhang. 2022. "Improved Landslide Susceptibility Mapping Using Unsupervised and Supervised Collaborative Machine Learning Models." <https://doi.org/10.1080/17499518.2022.2088802>.
- Takayabu, I., H. Kanamaru, K. Dairaku, R. Benestad, H. von Storch, and J. H Christensen. 2016. "Reconsidering the Quality and Utility of Downscaling." *Journal of the Meteorological Society of Japan* 94A:31–45. <https://doi.org/10.2151/jmsj.2015-042>.
- Taylor, K. E., R. J. Stouffer, and G. A Meehl. 2012. "An Overview of CMIP5 and the Experiment Design." *Bulletin of the American Meteorological Society* 93 (4): 485–498. <https://doi.org/10.1175/BAMS-D-11-00094.1>.
- Usovich, B., and J Lipiec. 2021. "Spatial Variability of Saturated Hydraulic Conductivity and Its Links with Other Soil Properties at the Regional Scale." *Scientific Reports* 11 (1): 1–12. <https://doi.org/10.1038/s41598-021-86862-3>.
- Weidner, L., T. Oommen, R. Escobar-Wolf, K. S. Sajinkumar, and R. A Samuel. 2018. "Regional-Scale Back-Analysis Using TRIGRS: An Approach to Advance Landslide Hazard Modeling and Prediction in Sparse Data Regions." *Landslides* 15 (12): 2343–2356. <https://doi.org/10.1007/s10346-018-1044-7>.
- Wu, W., and R. C Sidle. 1995. "A Distributed Slope Stability Model for Steep Forested Basins." *Water Resources* 31 (8): 2097–2110. <https://doi.org/10.1029/95WR01136>.
- Xgeo. n.d. "Varsom Xgeo." Date accessed March 18, 2023.
- Xiao, T., L. M. Zhang, R. W. M. Cheung, and S Lacasse. 2022. "Predicting Spatio-Temporal Man-Made Slope Failures Induced by Rainfall in Hong Kong Using Machine Learning Techniques." *Geotechnique*. <https://doi.org/10.1680/jgeot.21.00160>.

Appendix. Parametric hydrological analysis

Hydraulic parameters, such as conductivity, K [m s^{-1}] and diffusivity, D [$\text{m}^2 \text{s}^{-1}$], have very high importance in landslide susceptibility assessment because these parameters significantly affect the transient pore pressure build up, expressed in Equation (2), during the infiltration process. In this paper, the saturated hydraulic parameters, K_S and D_0 , were used because the saturated initial condition was assumed in TRIGRS model. These parameters depend on the soil texture, soil density, percentage of voids, grain size and distribution, etc., and significantly vary through space, even in the same geology unit. In the literature, a very high coefficient of variation, CoV which is the ratio of standard deviation to mean, was reported for K_S , such as 48.5–65.9% (Hu et al. 2008), 77.3% (Usovich and Lipiec 2021) based on the tests on a very large number of samples. Similarly, Liu and Wu (2008) reported the high variability of K_S and D_0 , and stated that D_0 values reported in the literature are in the range of (10–500) K_S .

A parametric hydrological analysis was performed via TRIGRS model to understand the effect of hydrological parameters on the transient pore pressure response. In the

parametric study, K_S values were used in the range from $1.0 \cdot 10^{-6} \text{ m/s}$ to $1.0 \cdot 10^{-4} \text{ m/s}$ with the ratio of $D_0/K_S \in [10, 200]$. For illustration purpose, the results of 1.5 m thick soil with 30° inclination are shown, although different slopes with varying thicknesses have been also investigated. In TRIGRS model, the initial ground water table was assumed at the bottom of the soil layer. The rainfall was simulated as a uniform spatial event during the rainfall duration and the pore pressure profiles were obtained at the beginning and at the end of the rainfall events.

For this parametric hydrological analysis, the IDF curves for the present climate condition were obtained by examining the historical time series from the weather station, Østås i Hegra. For the future climate condition, end of the twenty-first century (2071–2100), the ad-hoc IDF curves were obtained by a simple approach involved multiplying μ in Equation (1) with 1.4 to achieve a typical climate change scaling factor recommended by the Norwegian Climate Service Center (Dyrrdal and Førland 2019). This estimate of recommended climate change scaling factor is also in accordance with a simple and crude temperature-based scaling study for μ (Benestad et al. 2016). The rainfall depths are provided in Figure A1(a), and rainfall intensities are provided in Figure

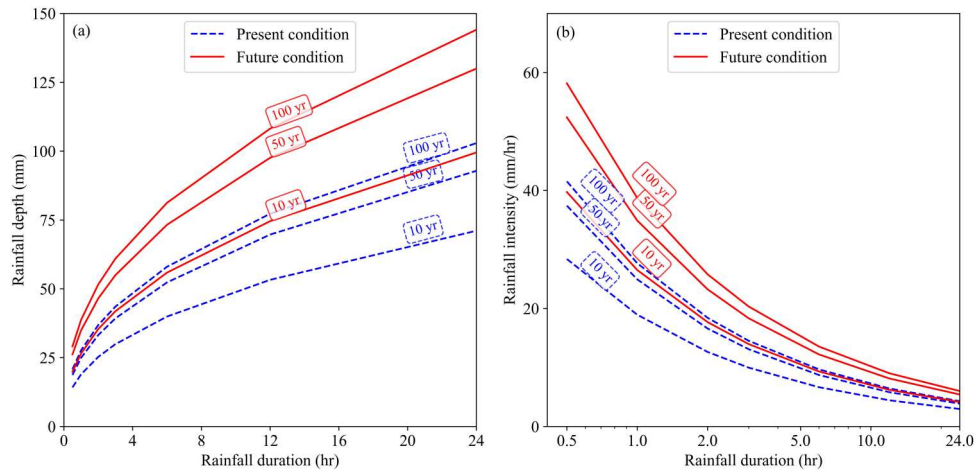


Figure A1. IDF curves for present conditions based on observations and ad-hoc IDF curves for future climate conditions using 1.4 climate change scale factor (return intervals, τ , are stated into boxes): (a) rainfall depth (b) rainfall intensity.

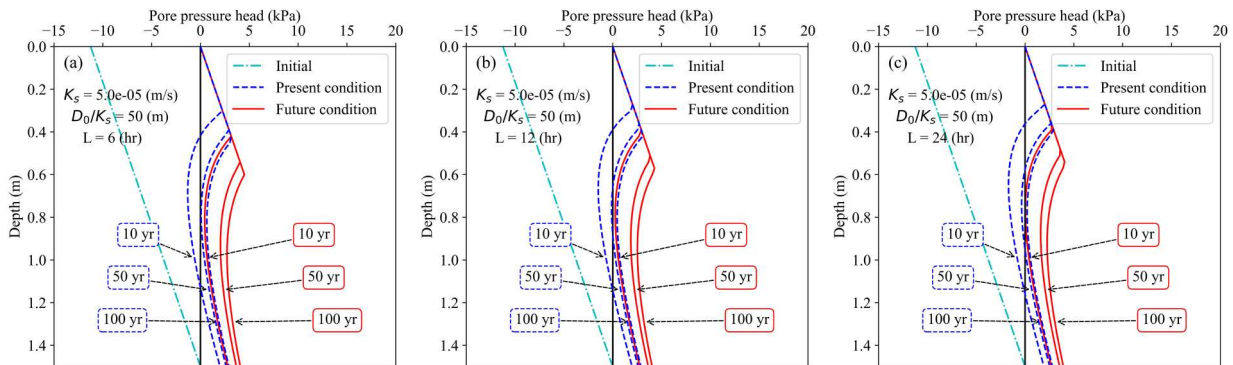


Figure A2. Effect of duration, L , on the transient pore pressure head response where $K_S = 5.0 \cdot 10^{-5} \text{ m/s}$, and $D_0/K_S = 50$: (a) 6-hour, (b) 12-hour, (c) 24-hour.

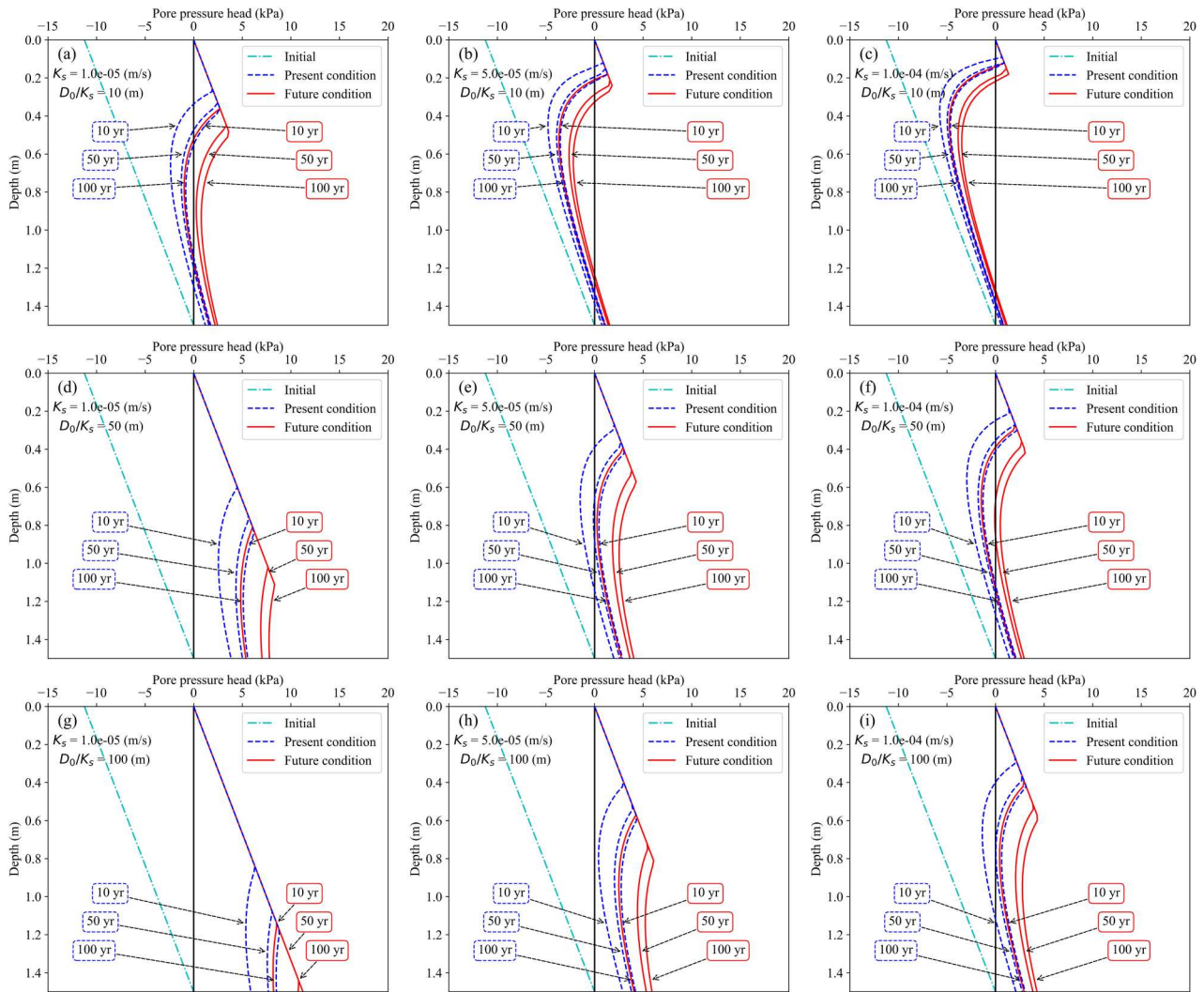


Figure A3. Effect of hydrological parameters on the transient pore pressure head response to a 12-hour rainfall event with return intervals of 10-, 50-, 100-year: (a, d, g) $K_S = 1.0 \cdot 10^{-5}$ m/s, (b, e, h) $K_S = 5.0 \cdot 10^{-5}$ m/s, (c, f, i) $K_S = 1.0 \cdot 10^{-4}$ m/s with D_0/K_S values of (a, b, c) 10, (d, e, f) 50, (g, h, i) 100.

A1(b) by dividing the rainfall depths by corresponding rainfall durations.

The analysis showed that different duration rainfall events of the same return interval, based on IDF curves, result in almost the same transient pore pressure response (Figure A2). This is attributed to the fact that the rainfall intensity Figure A1(b) changes with respect to the duration. Being longer duration and corresponding lower rainfall depths compensate for each other and similar transient pore pressure responses are obtained for different duration rainfall events of same return intervals.

Figure A3 shows the effect of hydrological parameters, K_S and D_0 , on the transient pore pressure response. For the illustration purpose, the results with K_S values of $1.0 \cdot 10^{-5}$, $5.0 \cdot 10^{-5}$, and $1.0 \cdot 10^{-4}$ m/s and D_0/K_S values of 10, 50, 100 are provided for 12-hour rainfall events of 10-, 50-, and 100-year return intervals (Figure A3). It can be seen that

higher K_S does not result in faster pore pressure build up because the water infiltrates faster into the soil and drains from the bottom. Figure A3 shows that a higher ratio of D_0/K_S results in a faster transient pore pressure response. The difference between the responses to different return intervals becomes wider when the ratio of D_0/K_S increases or K_S decreases.

The analyses showed that employing very low or very high values of D_0/K_S results in no considerable change in transient pore pressure response to rainfall events at present and future climate conditions. That is, low values of D_0/K_S results in very slow transient pore pressure especially for high values of K_S , and high values of D_0/K_S cause a fully saturation condition even at low intensity values. Therefore, employing such values of D_0/K_S would result in similar transient pore pressure response and similar landslide susceptibility assessments at present and future climate conditions.